Visual encoding signals around 200 milliseconds track onset of evidence accumulation during human decision making

Michael D. Nunez[1,2,*], Aishwarya Gosai[3,2], Joachim Vandekerckhove[2,4,5], Ramesh Srinivasan[2,1,5]

[1]*Department of Biomedical Engineering, University of California, Irvine, CA, USA*
[2]*Department of Cognitive Sciences, University of California, Irvine, CA, USA*
[3]*Massachusetts General Hospital and Harvard Medical School, Boston, MA, USA*
[4]*Department of Statistics, University of California, Irvine, CA, USA*
[5]*Institute of Mathematical Behavioral Sciences, University of California, Irvine, CA, USA*

Running title: Visual encoding signals around 200 milliseconds

[*]**Corresponding Author:**
Michael D. Nunez, PhD
Department of Biomedical Engineering
Henry Samueli School of Engineering
University of California, Irvine
Irvine, CA 92697
USA
Email: **mdnunez1@uci.edu**

Number of pages: 47

Number of figures: 9

Number of tables: 2

Number of words in Abstract: 249

Number of words in Introduction: 621

Number of words in Discussion: 1404

Conflict of interest statement: The authors declare no competing financial interests.

Acknowledgements: MDN, JV, and RS were supported by NSF grant #1658303. AG was supported by the Summer Undergraduate Research Program at the University of California, Irvine. Cort Horton and William Winter are well appreciated for creating useful MATLAB functions for EEG visualization and artifact removal. Siyi Deng and Sam Thorpe are thanked for their contributions to the FEM solutions and anatomical fMRI image generation. We would also like to thank Paul L. Nunez for his comments on the spline-Laplacian-localization technique used in this paper.

Author Contributions: MDN, JV, and RS designed research. AG and MDN performed research. MDN analyzed data. MDN, AG, JV, and RS wrote the paper.

Abstract

Previous research has shown that potentials collected from human electroencephalographic (EEG) records track evidence accumulation during perceptual decision making (O'Connell et al., 2012; Philiastides et al., 2014; Loughnane et al., 2016). However these studies relied on comparing differences across experimental conditions. In this study, we directly tested the hypothesis that N200 latencies (EEG stimulus-locked negative peaks occurring between 150 and 275 milliseconds in female and male human subjects) reflect visual processing time that occurs before evidence accumulation, labeled visual encoding time (VET), in the context of cognitive theory. Simulations of decision-making models show that differences in processes not related to evidence accumulation are tracked by early reaction time percentiles. The hypothesis that N200 latencies are analogs of VET was thus directly tested by quantifying 1-to-1 slope relationships in 1) linear regression between trial-averaged N200 latencies and early reaction time percentiles, 2) linear regression between single-trial N200 latencies and reaction times, and 3) parameter estimation of cognitive models of decision-making. Evidence was found of near 1-to-1 correspondence in each test. Deflection times of the N200 waveform were not found to have a significant relationship with early reaction time percentiles, suggesting that a certain threshold of initial extrastriate activity is necessary before evidence accumulation. N200 waveforms were projected to the cortical surface at temporal and extrastriate locations from a spline-Laplacian transformation, and are thus hypothesized to reflect the segregation from noise of the target stimulus. This research adds credence to the mounting evidence that N200 latencies track onset of evidence accumulation.

Key words: decision making; EEG; visual encoding time (VET); event related potentials (ERPs); diffusion models; hierarchical Bayesian methods

Significance Statement

Encoding of a sensory stimulus is the first step in perceptual decision making. In this manuscript we report evidence that human evoked potentials (EPs) around 200 milliseconds after stimulus presentation track the time of extrastriate cortical processing before visual evidence accumulation during decision making. These EP latencies vary across individuals and depend upon external visual noise. We present linear regressions, framed in the context of cognitive theory, to test 1-to-1 relationships between these EP latencies and reaction time distributions. Hierarchical Bayesian model-fitting was also used to relate these EPs to a specific cognitive parameter that tracks time related to visual encoding. This work adds to the growing literature that suggests that EEG records can track the onset of evidence accumulation.

Introduction

We define *visual encoding time* (VET) as the amount of time for visual processing to occur in the human brain before decision processes can begin. VET is expected to involve both top-down and bottom-up attention (see Desimone and Duncan, 1995) due to 1) the subject being in an environmental state where they may need to make a decision and 2) the subject's mind taking time to recognize the need for a quick response. VET is expected to be separate from the decision-related processing, which is often theorized to reflect a sequential accumulation of evidence (Ratcliff and McKoon, 2008). We may also expect there to be a difference between the initial response of the first neural populations in the cortex and a demarcation point where we reasonably expect decision-making to begin. That is, while there has been abundant evidence of visual information appearing in the primary visual cortex approximately 60 ms after stimulus onset (Schmolesky et al., 1998; Luck, 2012) this time may not reflect the time before evidence accumulation begins.

Experimental evidence for a sequential accumulation of information has been found on level of the neuron (Gold and Shadlen, 2007; Shadlen and Kiani, 2013), the level of the scalp-recorded electroencephalograph (EEG; O'Connell et al., 2012; Philiastides et al., 2014), and on the cognitive level (Voss et al., 2004; Ratcliff and McKoon, 2008). The time course of the evidence accumulation process, while varying dependent upon many factors such as the external signal quality and the participant themselves (O'Connell et al., 2012; Ratcliff and McKoon, 2008), could be as short as 30 ms in certain experimental paradigms (Stanford et al., 2010). Furthermore, much evidence exists for parallel decision-making and motor processing (Dmochowski and Norcia, 2015; Servant et al., 2015, 2016). However it can be reasonably expected that initial visual preprocessing, VET, must occur before any evidence accumulation or motor planning, representing a sequential processing step.

The processing speed of the human visual system has previously been estimated at about 150 milliseconds in humans with time-locked event related potentials (ERPs; Thorpe et al., 1996) using clever differences between conditions in go/no-go tasks. Loughnane et al. (2016) found initial evidence by looking at condition differences to suggest that stimulus-locked negative peaks around 200 milliseconds (N200) influence the onset of a neural correlate of evidence accumulation. In another study, single-trial EEG potentials thought to be generative of N200 peaks were suspected to

be related to a "preattentive" phase of decision-making, reflecting the time for attended visual information to reach the extrastriate areas (Zhang et al., 2016). Single-neuron recordings of evidence accumulation from lateral intraparietal areas (LIP) in primates typically begin at similar time periods after an experimental stimulus is displayed (Shadlen and Kiani, 2013). Finally, Martin et al. (2010) found that both 1) N200 deflection time and 2) the difference between N200 peak-latency and N200 deflection time were positively correlated with non-decision time (NDT; the sum of time-invariant processes across trials not associated with a sequential accumulation of evidence).

In this study, we sought to verify that N200 deflection times and N200 peak-latencies tracked visual encoding time (VET) using novel approaches to estimate cognitive models of perceptual decision making. First we propose a new way of estimating traditional EEG measures to track subjects' VET. We then found evidence that stimulus-locked N200 peak-latencies track VET at a 1 millisecond to 1 millisecond correspondence using data from decision-making tasks. We also find similar evidence for this relationship using linear regression analyses; analyses that relax assumptions about the underlying theoretical neural and cognitive models. These results suggest that N200 peak-latencies reflect human visual encoding time (VET) while N200 deflection times do not. This study extends initial work presented in Chapter 4 of the PhD dissertation by Nunez (2017).

Materials and Methods

Session-level observations

In order to evaluate the hypothesis that N200 latencies track VET, data was analyzed from two similar experiments. Data from Experiment 1 consisted of EEG recordings and behavioral observations from 12 unique subjects (3 female, 9 male) with 2 sessions of EEG each. Data from Experiment 2 consisted of EEG recordings and behavioral observations from 4 unique subjects (2 female, 2 male) with 7 sessions each. Two male subjects participated in both experiments resulting in 14 unique subjects across both experiments (5 female, 9 male) with 52 unique EEG sessions. All subjects gave written informed consent, and all data was collected at the University of California, Irvine with approval and recommendations from the Internal Review Board. All subjects had normal or corrected-to-normal vision and had no history or family history of epilepsy. Sessions of EEG collection and task performance for each subject in Experiment

1 were separated by at least 24 hours. Sessions of EEG collection and task performance for each subject in Experiment 2 were separated by 1 week. Session-level linear regressions and direct cognitive model fits treat all EEG sessions as observations for the regression relationships between N200 peak-latency and VET estimates. While subject differences are important and explored below, observations were collapsed across EEG sessions because our hypothesis was that N200 peak latencies would track VET no matter the external visual noise condition, subject, or subject's internal state that changed across EEG sessions.

Experimental tasks

Subjects were tasked to perform a two-alternative forced choice task, specifically to determine whether a Gabor stimulus contained high or low spatial frequency content. Stimuli for Experiments 1 and 2 are built and displayed using the MATLAB Psychophysics toolbox (Psychtoolbox-3; www.psychtoolbox.org). Example stimuli for both Experiments 1 and 2 are given in **Figure 1**).

Subjects in the two experiments performed perceptual decision making tasks in a dark room on a 61 cm LCD monitor maintaining a distance of approximately 57 cm from retina to display. The monitor resolution was set as $1920 * 1280$ pixels with a 120 Hz refresh rate. Visual angle refers to the angular distance from a stationary subject's retina to an object in the visual field. A distance of 57 cm was chosen to ensure easy calculation of visual angles, with x cm approximately equaling x° visual angle. The subjects were told to remain fixated on a small fixation spot while performing the task.

Gabors are spatial grating patterns with a Gaussian falloff of contrast that produces maximal firing in certain neurons within the primary visual cortex (Webster et al., 1985). Subjects in both experiments were tasked with identifying the spatial frequency (either "high" or "low" spatial frequency) of large Gabors that were randomly rotated and at a random phase on each trial, matching observed Gabor templates (observed by the subjects as stationary pictures before the first session) with the spatial frequency observed on the current trial. In Experiment 2, the high and low spatial frequencies of the target Gabors were 2.4 and 2.6 cycles per degree visual angle (cpd) respectively. While in Experiment 1, the targets were randomly drawn from a $\mathscr{B}eta(13.5, 1.5)$ distribution or a $\mathscr{B}eta(1.5, 13.5)$ distribution

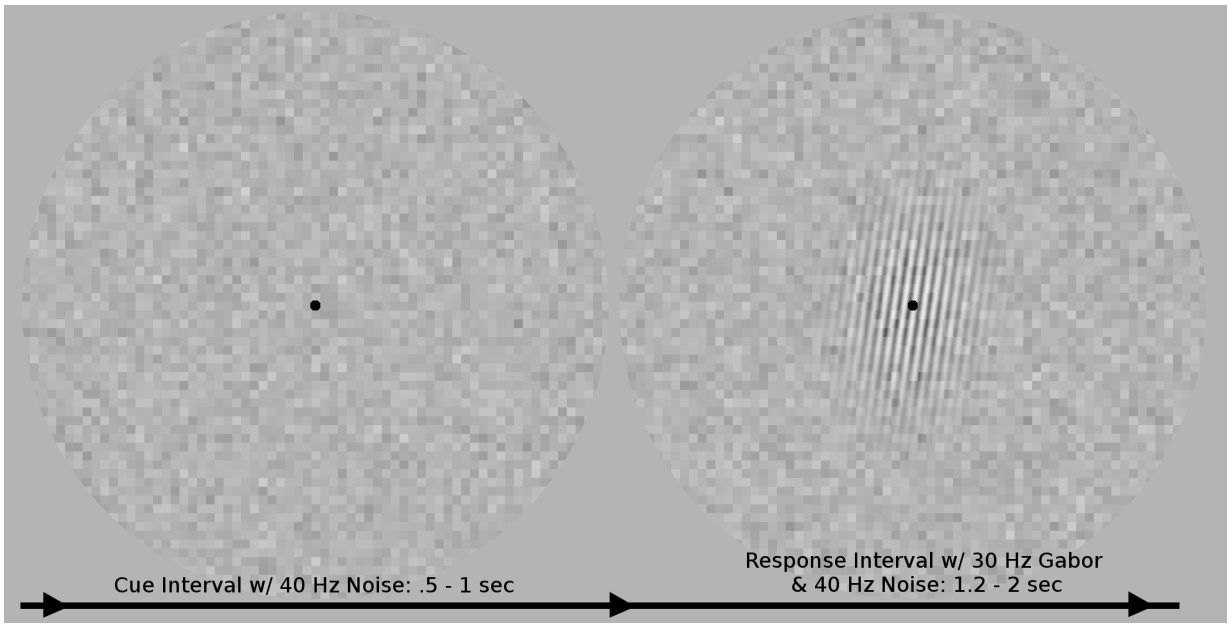

(a) Experiment 1

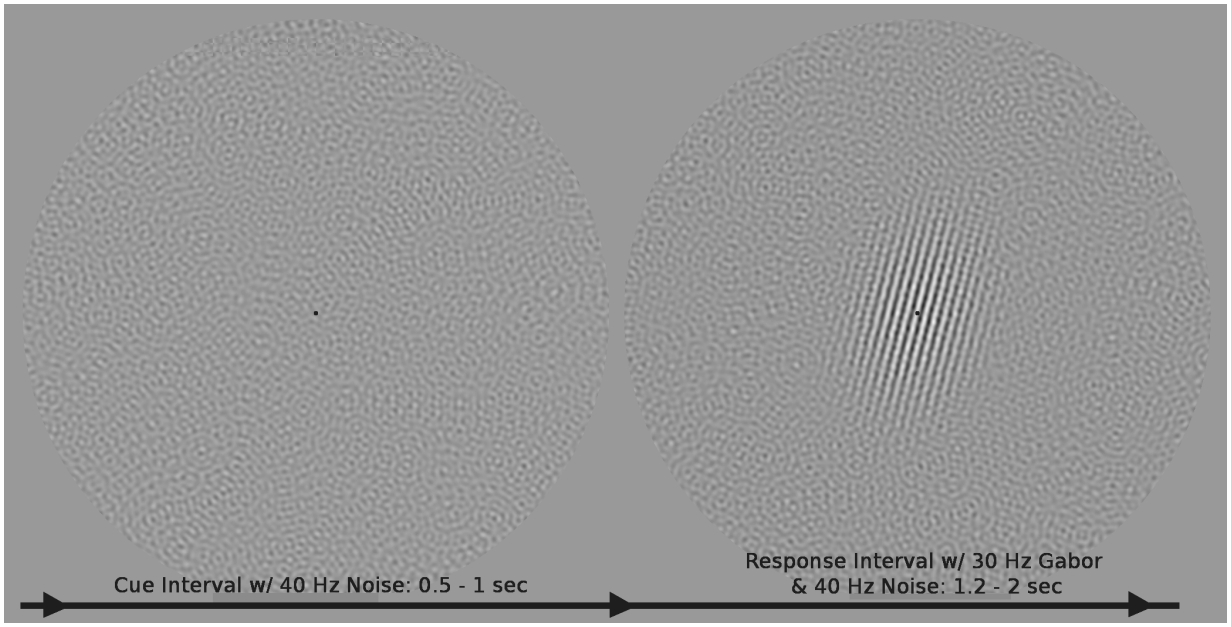

(b) Experiment 2

Figure 1. Example stimuli of the *cue* and *response* intervals of medium noise conditions from Experiments 1 (top) and 2 (bottom). During the response interval, subjects decided which spatial frequency each target Gabor matched, pressing a button with their left hand for a low spatial frequency target (2.4 cycles per degree visual angle, cpd) and pressing a button with their right hand for a high spatial frequency target (2.6 cpd). N200 waveforms were calculated time-locked to the onset of the Gabor stimulus during the response intervals. In both experiments a paradigm was used in which the visual noise changed at 40 Hz and the Gabor signal flickered at 30 Hz to evoke 40 Hz and 30 Hz responses in electrocortical activity that track attention to the noise and signal stimuli. While the attention analysis is not discussed in this paper, a similar analysis is presented by Nunez et al. (2015).

with means 2.4 and 2.6 cpd respectively. Before and during the Gabor display on each trial, a disk of visual noise was displayed. In Experiment 1, checkerboard noise was displayed. While in Experiment 2, the noise was spatially bandpass filtered to include only masking noise centered around 2 and 3 cpd, equally masking both the high and low spatial frequency targets. Both experiments contained three conditions of high, medium, and low visual noise contrast.

The time course of each trial was as follows: subjects were asked to fixate on a small fixation spot in the center of the screen throughout the experiment, visual noise changing at 40 Hz was displayed a variable length of time between 500 ms to 1000 ms during the *cue* interval, then the Gabor signal stimulus was flickered at 30 Hz embedded in the noise stimuli for 1200 ms to 2000 ms during the *response* interval. During the response interval, subjects are asked to respond as accurate as possible in the time allowed using a button box (using their left hand to respond for low spatial frequency targets and their right hand for high spatial frequency targets). Auditory feedback was given after the response interval indicating trial accuracy, which was included in order to encourage subject vigilance. An entire session of task performance and EEG collect took subjects approximately 1 hour with breaks. Each session produced 8 blocks of 60 trials each for a total of 480 trials, with the noise contrast conditions intermixed within each block. Subjects were allowed to take breaks between blocks.

EEG recording

EEG was collected in both experiments using Electrical Geodesic, Inc.'s 128 electrode sensor net and a Net Amps 200 series amplifier. Electrical activity from the scalp was recorded at a sampling rate of 1000 samples per second and hardware bandpass filtered to either 1 to 50 Hz (EEG data from Experiment 1) or 1 to 100 Hz (EEG data from Experiment 2). The hardware band pass filter in Experiment 2 was chosen purposely to maintain high frequencies so that broadband noise is submitted to an Independent Component Analysis (ICA) in order to aid artifact correction (i.e. removing electrical activity due to muscle, movement and environmental electrical influence, see Makeig et al., 1996; Nunez et al., 2016). However both analyses yielded artifact-resistant measures after ICA that were used for further processing as detailed below.

Calculation of N200 waveforms

N200 waveforms, calculated from event-related potentials (ERPs) to the onset of the Gabor patch during the *response* interval were obtained using five processing steps: 1) low pass filtering the EEG data to obtain cleaner estimates of evoked potentials, 2) shifting each trial's amplitude to rereference to a baseline (i.e. the average amplitude in a 100 ms window before the stimulus), 3) averaging across trials to obtain a traditional ERP estimate at 128 electrodes for each subject (minus those electrodes marked as artifactual), 4) taking a singular value decomposition (SVD) of the ERPs, and then 5) using the first component (the component that explained the most variance) as an channel weighting function in order to obtain a less-noisy estimate of the N200 waveforms for both EEG session in each visual noise on single trials.

The goal of the singular value decomposition (SVD) was to improve the signal-to-noise ratio of both traditional ERP estimates and single-trial estimates by weight-averaging adjacent electrodes as a spatial filter (Kayser and Tenke, 2003; Parra et al., 2005). SVD is the algorithm used my most principal component analysis (PCA) algorithms and produces non-stochastic, deterministic results. N200 waveforms were obtained by finding the first principal component of the matrix of ERPs (samples T by channel C data, see Methods in Nunez et al., 2017). The first principal component consists of both a weight vector that produces a time series over of the trial-average and an associated vector of weights representing the location of that component. Single-trial estimates of that ERP are then obtained by weight-summing over the vector of weights as described by Nunez et al. (2017) and **Figure 2**. It should be noted that the *first* component of the SVD method only pulled out the N200 waveform because 1) the stimulus was large and therefore the neural response to the visual stimulus was large and 2) there were only small P300 responses. Had the experimental conditions been different, the N200 waveform may have been placed in a SVD component that explained less of the variance. Traditionally calculated ERPs at specific parietal electrodes were also compared to the trial-averaged method yielding no difference in latency calculations (Luck, 2012).

Different methods for finding channel weights for single-trial estimation of N200 latencies were explored. The best method was quantified as the method that produced clear peaks at typical N200 latencies over all trials. The following methods were explored in depth: 1) calculating ERPs in each SNR condition and biasing single-trial

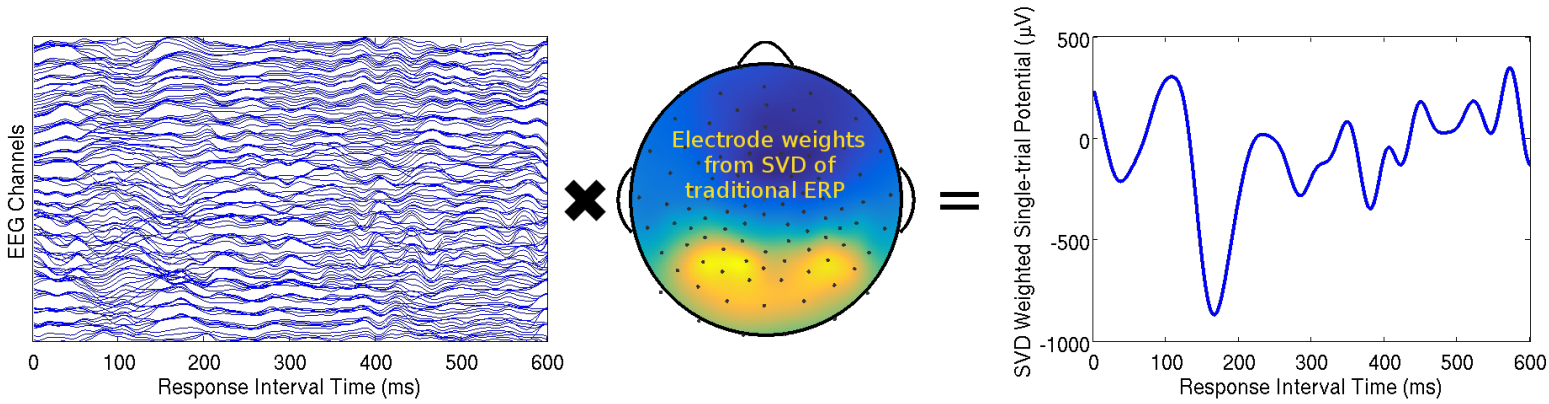

Figure 2. A visual representation of the singular value decomposition (SVD) method for finding single-trial estimates of evoked responses in EEG. The EEG presented here is time-locked to the signal onset during the response interval, such that the single-trial N200 waveform encoded the response to the signal onset. A single trial of EEG from one subject (Left) can be thought of as a time by channel ($T \times C$) matrix. The first SVD component explained the most variability in this subject's ERP response to the signal across all trials in the training set. SVD weights $\mathbf{v}$ ($C \times 1$) are obtained from the ERP response (i.e. trial-averaged EEG; $T \times C$) and can be plotted on a cartoon representation of the human scalp with intermediate interpolated values (Middle). This specific trial's N200 waveform (Right) was obtained by multiplying the time series data from each channel on this trial by the associated weight in vector $\mathbf{v}$ and then summing across all weighted channels. Weight averaging across channels is a common method to obtain larger signal-to-noise ratios in EEG (e.g. cleaner, more task-relevant neural signals, see Parra et al., 2005).

EEG in each condition using an SVD component based on that conditions average, 2) calculating ERPs only in the low noise condition and biasing single-trial EEG in each condition using an SVD component based only on the low noise condition, or 3) calculating ERPs across all trials, disregarding condition, and biasing single-trial EEG by that SVD component. Method 1 was found to be the best calculation. An Independent Component Analysis (ICA) decomposition of ERP response matrix $T \times C$ was also explored. However independent components (ICs) did not produce consistent estimates of components across subjects. Thus the SVD was found to be a more stable and objective calculation when the first component from each subject and condition was used.

The window to calculate minima in order to evaluate N200 peak-latency responses was found empirically. Out of the following windows: 100 to 300 ms post-stimulus, 100 to 250 ms post-stimulus, 150 to 225 ms post-stimulus, and 150 to 275 ms post-stimulus, the 150 to 275 ms window post-stimulus was found to capture the N200 waveform on the subject-level well in each condition because few edge-located minimums were detected in the trial-averaged N200 peak-latency estimates (i.e. because only 3 estimates out of 147 estimates of trial-averaged N200 peak-latency were detected at the boundary, it was thought that his window well captured the N200 waveform). If either trial-averaged or single-trial N200 peak-latencies were found with a minimum on the boundary, they were removed from the analysis. A minimum at either 150 or 275 ms was indicative that N200 latencies were not well estimated in that noise condition or on that trial.

Deflection times were also calculated for the trial-averaged N200 waveforms by taking the window of 0 to 275 ms post-Gabor onset in the response interval and finding were the derivative of the ERP in that window first became negative before the N200 peak-latency. This reflects the point at which the signal begins to decrease before the N200 peak-latency. This is hypothesized to be a time point of early visual processing and was tested by regressing against VET estimates. This particular time point has been explored in a previous study of visual encoding by Martin et al. (2010), albeit calculated using the point at which the signal reached two standard deviations below the baseline. Trial-averaged N200 waveforms and deflection time and peak-latency distributions are shown in **Figure 3**.

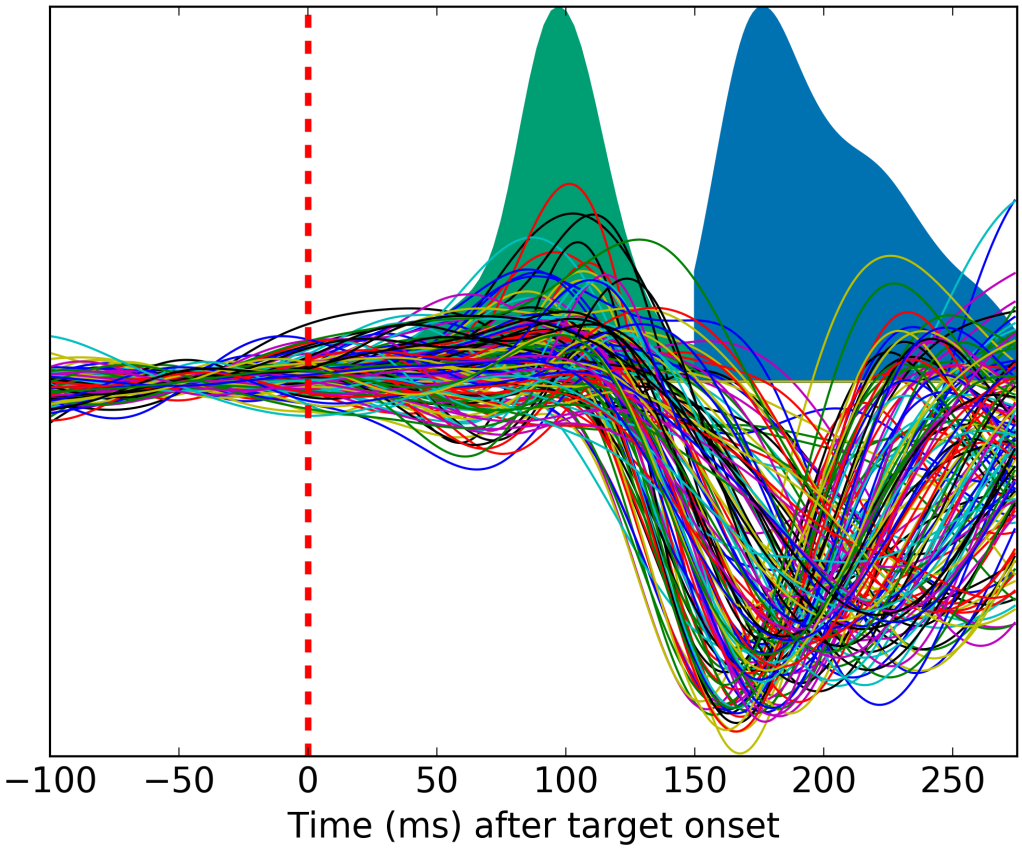

Figure 3. All trial-averaged N200 waveforms across EEG sessions and the 3 visual noise experimental conditions ($N = 147$). Smoothed histograms for the N200 deflection times (green distribution) as well as the N200 peak-latency times (blue distribution) are also displayed above. There was a significant but weak correlation found between the found N200 deflection times and the N200 peak-latency times ($\rho = .274$). N200 deflection times are not as variable across EEG sessions and noise conditions as N200 peak-latencies.

Presence of fast errors in reaction time distributions

One possible confound in evaluating the relationship between N200 latencies and reaction time distributions is the presence of fast error reaction times. That is, fast reaction time observations that are not due to a decision making process, and occur due to another random process (e.g. a "contaminant" process unrelated to the theorized cognitive process). Because these reaction times are not due to a decision process, the associated accuracy on those trials should be about 50% in a two-alternative forced choice task. Recent research has studied and developed theory on the notion of "mind-wandering", which is defined as cognition that departs from that which is useful to the task at hand (e.g. Hawkins et al., 2015; Fox et al., 2015; Lin et al., 2016). Fast errors could be considered a special case of mind-wandering, contaminant trials. An analysis of other types of contaminant trials and the influence of these trials on the presented analyses is discussed below.

In order to remove fast responses times that were not due to a decision process, an exponentially weighted moving average was used to calculate accuracy sorted by reaction time, from shortest reaction time to longest reaction time. A cutoff of 60% accuracy was used and the accuracy data and the associated short reaction times were removed from the data. However a fixed cutoff of 350 ms yielded no difference in the ultimate results, and therefore a fixed cutoff was maintained in the data. This procedure resulted in less than 7.6% of the response data being dropped for each visual noise condition across sessions of EEG, with the median being 0% removed in one visual noise condition of one session.

Cognitive model justification

We tested our hypothesis directly by fitting reaction time and choice data from the human subjects to simple decision-diffusion models. In these models, human *visual encoding time* (VET) is the first cognitive processing time after a visual stimulus is displayed and the subject must make a decision based on the visual input (see **Figure 9**). The *non-decision time* (NDT) τ parameter is the sum of VET and other time-invariant processes across trials not associated with a sequential accumulation of evidence, such as motor execution time. We therefore tested whether the linear relationship between N200 peak-latency and NDT had a slope of 1, reflecting the hypothesis that N200 peak-latency is one additive

component of NDT.

We assess our ability to recover true non-decision time (NDT) estimates from RT percentiles and hierarchical Bayesian model fitting by simulating reaction time data. Reaction time data was simulated from decision-diffusion models with various amounts of trial-to-trial variability across EEG sessions in NDT, evidence boundary (amount of evidence require to make a decision), and evidence accumulation rate (i.e. drift rate) suggested by Ratcliff (1978). These reaction times were simulated using DMAT, MATLAB software for simulating and estimating diffusion model parameters (Vandekerckhove and Tuerlinckx, 2008). These simulations revealed that even with the presence of trial-to-trial variability in NDT, evidence boundary, and evidence accumulation rate, means of non-decision time and evidence accumulation rate could still be recovered. In particular, mean NDT across trials was well estimated by 1) 10th percentiles of reaction time distributions (with about 60 milliseconds of fixed bias in 10th percentiles compared to true mean NDTs) and 2) hierarchical Bayesian fitting of a simple decision-diffusion model (DDM) with inter-trial variability in the three free parameters (Wabersich and Vandekerckhove, 2014). Although mean NDTs are not as well estimated in the presence of a large amount of contaminant trials (see Results section and **Figure 7**). This means that embedded regression analyses will reflect true relationships between N200 waveforms and cognitive parameters, assuming that the theoretical model of decision making approximates the true cognitive process.

N200 waveforms versus reaction time

Linear regressions of trial-averaged N200 deflection times and peak-latencies versus reaction time percentiles across EEG sessions and noise conditions and single-trial N200 peak-latencies versus reaction times were performed. The fastest reaction times in each EEG session and noise condition are expected to be the linear sum of *visual encoding time* (VET) and other sequential cognitive processes (that mostly invariant across trials). This is because in any reaction time process that contains a mix of stochastic evidence accumulation and fixed processes with smaller amounts of variability, NDT (time periods not associated with evidence accumulation during decision making trials, see Voss et al., 2004; Ratcliff and McKoon, 2008) will be reflected in the fastest reaction times. The fastest reaction times in each EEG session and noise condition were estimated by the 10th percentile. The 10th percentile was chosen because

the smaller percentiles were suspected to include contaminants due to mind-wandering as discussed above (although similar results were empirically found in post-hoc analyses of the 1st percentile RTs).

Linear regression statistics reported are 95% confidence intervals related to the p values and t statistics in the Neyman and Pearson (1933) tradition as well as Bayes Factors (BF) which describe the amount of relative evidence (probability in the Bayesian definition) of a model which has a non-zero regression slope over a model which has a regression slope of zero (Jeffreys, 1961; Kass and Raftery, 1995; Rouder and Morey, 2012). Generally Bayes Factors over 3 are considered positive evidence for an effect (i.e. the effect is 3 times more likely under the alternative hypothesis than the null hypothesis) while over 20 is strong evidence (Kass and Raftery, 1995). BF reported here were very large and therefore the natural logarithm of the Bayes Factor, $\log(\mathrm{BF})$ is reported. Adjusted R^2 is also reported that describes the fraction of variance of the dependent variable (RT statistics) explained by the regressor variable (measures of neural processing speed). R^2_{adj} ranges from 0 to 1. These statistics were generated by JASP, a open-source graphical software package for statistical analysis (JASP Team, 2017).

Also reported are Bayes Factors (BF1) of a 1-to-1 relationship between reaction time and N200 measures that describe the amount of relative evidence (e.g. "probability" in the Bayesian definition) of the slope parameter being equal to 1 (e.g. 1 ms increase in N200 peak-latency corresponds to a 1 ms increase in visual encoding time) over a model which has a largely unknown regression slope such that the comparison density and prior probability of slope parameter β was $\beta \sim \mathcal{N}(1, 3^2)$. BF1 were calculated using the simple Savage-Dickey Density Ratio (Dickey et al., 1970; Wagenmakers et al., 2010) which is the ratio of the height of the posterior distribution over the prior distribution that are both centered on the tested value. These Bayes Factors were calculated by running simple JAGS code, a program that easily samples from marginal posterior distributions of using Markov Chain Monte Carlo (MCMC) (Plummer, 2003). These Bayes Factors, BF1, are on a different scale than the Bayes Factors used to test the existence of an effect, $\log(\mathrm{BF})$, because less data is needed to prove the existence of an effect than to prove the effect is equal to a specific value (slope equal to 1, in this case).

Integrated neurocognitive model fitting

Testing the data directly, parameter estimates from three hierarchical Bayesian models were found. These linear relationships were estimated in a single-step in a hierarchical Bayesian framework.

Decision-diffusion modeling was applied to reaction time and accuracy data from Experiments 1 & 2 jointly, containing between session-differences in NDT τ, evidence accumulation rate δ, and speed accuracy trade-off parameter α that were explained by session j and condition k differences in N200 waveform peak-latencies ζ_{jk}. All built models will were assumed to be hierarchical, describing intrinsic session j and condition k variability which 1) ensured model fits with small amounts of data (Lee, 2008; Lee and Newell, 2011; Vandekerckhove et al., 2011) and 2) provided the ability to predict data more easily for observed and unobserved subjects in future analyses (Wagenmakers, 2009; Nunez et al., 2017). Hierarchical parameters were also split by experiment e. Bayesian hierarchical decision-diffusion models were fit using Wiener likelihood approximations in JAGS, which can easily sample from hierarchical models using Markov Chain Monte Carlo (MCMC) (Plummer, 2003; Wabersich and Vandekerckhove, 2014), with pyjags in Python (Miąsko, 2017).

Models 1 and 2 had the same base structure on decision-diffusion model parameters with linear regression influence of N200 peak-latency z_{jke} on each parameter, expressed as functions $f(z_{jke})$. Model 3 had the same base structure with function $f(z_{jke}) = 0$ on the session j level but single-trial regressions on the trial n level discussed below, The base structure of all three models was the following:

$$
\begin{aligned}
\tau_{jke} &\sim \mathcal{N}(\eta_{(\tau)ke} + f_1(z_{jke}), \sigma^2_{(\tau)}) \in (0,1) \quad , \quad \eta_{(\tau)ke} \sim \mathcal{N}(0.3, 0.25^2), \quad \sigma_{(\tau)} \sim \Gamma(0.2,1) \\
\delta_{jke} &\sim \mathcal{N}(\eta_{(\delta)ke} + f_2(z_{jke}), \sigma^2_{(\delta)}) \in (-9,9), \quad \eta_{(\delta)ke} \sim \mathcal{N}(1, 2^2) \quad , \quad \sigma_{(\delta)} \sim \Gamma(1,1) \\
\alpha_{jke} &\sim \mathcal{N}(\eta_{(\alpha)ke} + f_3(z_{jke}), \sigma^2_{(\alpha)}) \in (0.1,3), \quad \eta_{(\alpha)ke} \sim \mathcal{N}(1, 0.5^2) \quad , \quad \sigma_{(\alpha)} \sim \Gamma(1,1) \\
z_{jke} &\sim \mathcal{N}(\zeta_{ke}, \sigma^2_{(z)}) \quad , \quad \zeta_{ke} \sim \mathcal{N}(0.2, 0.1^2) \quad , \quad \sigma_{(z)} \sim \Gamma(0.2,1)
\end{aligned}
$$

In Model 1, wide (uninformative) priors were given to the hierarchical effects μ_i of N200 peak-latency on decision-diffusion model parameters i, centered at 1 in order to calculate Bayes Factors (BF1) testing a 1-to-1 relationship using the Savage-Dickey density ratio (Verdinelli and Wasserman, 1995). As a sensitivity analysis, wide priors centered at 0

were used in previous fits of the model that only had inconsequential effects on the parameter estimates (i.e. posterior distributions). The final fit of Model 1 thus had the following embedded linear regression and prior structure:

$$f_i(z_{jke}) = \gamma_{ike} z_{jke}$$

$$\gamma_{ike} \sim \mathcal{N}(\mu_i, \sigma^2_{(\gamma)}), \quad \mu_i \sim \mathcal{N}(1, 3^2), \quad \sigma_{(\gamma)} \sim \Gamma(1,1)$$

Model 2 was created in order to test the post-hoc hypothesis that noise condition and visual noise type (differing across the two experiments) modified the effect of N200 peak-latency on NDT. In Model 2, the effect of trial-averaged N200 peak-latency on NDT was assumed to be moderated by noise condition and experiment. The modifying effects tested were the effect of any additional visual noise above low noise θ_{i1}, the effect of high noise θ_{i2}, the effect of Experiment 2 θ_{i3}, the interaction effect between any additional noise and Experiment 2 θ_{i4}, and the interaction effect between high noise and Experiment 2 θ_{i5}. Priors of the modifier effects θ of N200 peak-latency on the decision-diffusion model parameters were centered at 0 in order to calculate Bayes Factors for support of the null hypothesis (BF0) using the Savage-Dickey density ratio (Verdinelli and Wasserman, 1995). Thus Model 2 had the following embedded linear regression and prior structure:

$$f_i(z_{jke}) = \gamma_{ike} z_{jke} + \theta_i{}^{\mathsf{T}} \mathbf{z}_{jke} = \gamma_{ike} z_{jke} + \theta_{i1} z_{jke} + \theta_{i2} z_{jke} + \theta_{i3} z_{jke} + \theta_{i4} z_{jke} + \theta_{i5} z_{jke}$$

$$\gamma_{ike} \sim \mathcal{N}(1, 3^2), \quad \theta_{iike} \sim \mathcal{N}(0, 1^2)$$

In **Model 1** Bayes Factors for effect parameters in each experiment and condition were calculated with Python and R scripts using a Savage-Dickey density ratio (Verdinelli and Wasserman, 1995) of the posterior density over the prior distribution at $\gamma = 1$. These Bayes Factors provide the degree of evidence (defined as a probability ratio in Bayesian

statistics) of a model where effect of trial-averaged N200 peak-latency on NDT is 1-to-1 versus a model where the effect is unknown (the prior model where $\gamma \sim \mathcal{N}(1, 3^2)$). In **Model 2** Bayes Factors for *additional* effect parameters in each experiment and condition were calculated using a Savage-Dickey density ratio of the posterior density over the prior distribution at $\theta = 0$, i.e. the null model of no additional N200 effect with increasing visual noise contrast. These Bayes Factors provide the degree of evidence of a model where effect of trial-averaged N200 peak-latency on NDT is 0 versus a model where the effect is unknown (the prior model where $\theta \sim \mathcal{N}(0, 1^2)$).

Model 3 was fit to find posterior distributions of decision-model parameters for *single-trial* N200 peak-latency linear effects on single-trial NDT (the sum of encoding and motor response time as estimated by a hierarchical Bayesian account of a decision-diffusion model). Because of the expected presence of mind-wandering, the results of model fitting simulation, and known caveats with this modeling method (e.g. see Hawkins et al., 2017), it was expected that while the model may uncover a true positive relationship, we would not be able to recover the true effect size with linear parameters. The model was fit with linear relationships between N200 peak-latencies x on single-trials n and single-trial decision-diffusion model parameters (with an exponential around the boundary separation linear equation in order to aid in model fitting, reflecting a multiplicative effect on boundary separation instead of a linear effect). Also included were hierarchical linear effect parameters in order to summarize the linear effects at certain noise conditions. In addition to the base structure presented at the beginning of this section, Model 3 had the following structure (where $\mathbf{y}$ refers to the choice and reaction time on trial n from a decision-diffusion model; DDM):

$$f_i(z_{jke}) = 0$$

$$\mathbf{y}_{njke} \sim \mathrm{DDM}(\tau_{jke} + \lambda_{1jke} x_{njke},\ \delta_{jke} + \lambda_{2jke} x_{njke},\ \exp(\alpha_{jke} + \lambda_{3jke} x_{njke}))$$

$$x_{njke} \sim \mathcal{N}(z_{jke}, \sigma^2_{(x)}), \quad \sigma_{(x)} \sim \Gamma(0.2, 1)$$
$$\lambda_{ijke} \sim \mathcal{N}(\gamma_{ike}, \sigma^2_{(\lambda)}), \quad \sigma_{(\lambda)} \sim \Gamma(1, 1)$$

$$\gamma_{ike} \sim \mathcal{N}(\mu_i, \sigma^2_{(\gamma)}), \quad \mu_i \sim \mathcal{N}(1, 3^2), \quad \sigma_{(\gamma)} \sim \Gamma(1, 1)$$

Source localization of N200 peaks

While EEG localization is an inexact process that is unsolvable without additional assumptions, the surface spline-Laplacian (i.e. Current Source Density, CSD) has been shown to match closely to simulated cortical activity using forward models (i.e the mapping of cortical activity to scalp potentials), are unaffected by reference electrode choices, and have shown consistent results when used with real EEG data (Nunez and Srinivasan, 2006; Kayser and Tenke, 2015). In addition, unlike 3D solutions, projections to dura mater surface are theoretically solvable, and have been used with success in past studies (see Nunez et al., 1994, for an example). Repeating a similar "source-localization" technique found in Nunez et al. (2017), we localized a 2D surface spline-Laplacian (Deng et al., 2012) to the gyral crowns of a folded cortical surface (i.e. the "smooth" cortex). In forward model solutions of simulations, Nunez and Srinivasan (2006) found that the contribution to surface EEG amplitude is about three times as much by smooth gyral surfaces than sulcal surfaces. Furthermore, Nunez and Srinivasan (2006) found that two parallel sulcal surfaces can cancel each other's contribution to the scalp EEG potential. These two empirical findings suggest that while the true sources of the N200 waveform would be found in sulcal walls of the extrastriate, this is less likely than the sources being in the gyral crowns of the extrastriate.

We first found surface spline-Laplacians on the realistic MNI average scalp (Deng et al., 2012) of the trial-averaged N200 waveforms for each subject. The surface Laplacians were then projected onto a cortical shape generated by an anatomical MRI of a subject that did not participate in this study. This subject's brain image had cortical folds that better localized particular regions than the MNI brain shape. We hold the opinion that this method more accurately represents an image of a cortex than the MNI brain. Each subject's N200 projection was performed using Tikhonov (L2) regularization and a Finite Element (FE; Pommier and Renard, 2005) forward model to the MNI 151 average head, maintaining similar spatial-distributions of activity of the surface Laplacians to the cortical surface from the scalp (or dura) surface. Each localization was then labeled using the Destrieux cortical atlas (Fischl et al., 2004)

by using a cutoff of -10 microamperes per mm^2. Locations listed were ones that were found in at least 60% of localizations across EEG sessions and experimental conditions. However we should note that the exact localization must have some errors due to between-subject variance in both cortical and cranial shape and between-subject variance in tissue properties. These sources of variance could not easily be accounted for, and remains a source of error in this (and all) cortical projection techniques.

Code Accessibility

Pre-calculated EEG measures, raw behavioral data, MATLAB stimulus code, MATLAB, Python, R, and JAGS analysis code are available on `https://osf.io/jg9u3/` and in the following repository `https://github.com/mdnunez/encodingN200` (as of March 2018).

Results

N200 deflection, peak-latency, reaction time and accuracy distributions

After removal of suspected poorly-estimated N200 peak-latencies (e.g. latencies found at either the 150 or 275 millisecond boundaries) and removal of some contaminant trials (reaction times smaller than 350 milliseconds), data summarizes of N200 deflection times, trial-averaged N200 peak-latencies, 10th reaction time percentiles (thought to be a stable but biased estimate of NDT), median reaction times across trials, and mean accuracy across trials are given in **Table 1**, such that the total sample size of each measure was $N = 147$. A significant but weak correlation was found between the found N200 deflection times and the N200 peak-latencies ($\rho = .274$, $p < .001$). A significant correlation was found between the N200 peak-latencies and 10th reaction time percentiles (a less specific test of our main hypothesis; $\rho = .387$, $p < .001$). No correlation was found between the N200 deflection times and 10th reaction time percentiles (a less specific test of our secondary hypothesis; $\rho = -0.09$, $p = .30$).

There were 14 unique subjects across both experiments (with two subjects participating in both experiments). In order to explore true individual differences, observations of the N200 deflection time, N200 peak-latency, median reaction time and accuracies were averaged across the two experiments and all conditions for each subject. The range of these

Data summary across unique EEG sessions ($N = 49$) and conditions (total $N = 147$)

		N200 Deflection times	N200 Peak-latencies	10th Percentile Reaction times	Median Reaction times	Mean Accuracy
	Overall Mean	95.5 ms	199.6 ms	575.0 ms	852.8 ms	78.76%
	5th Percentile	48.3 ms	162.0 ms	443.6 ms	629.5 ms	58.36%
	Median	97.0 ms	192.0 ms	562.4 ms	845.8 ms	78.76%
	95th Percentile	136.5 ms	259.8 ms	733.6 ms	1139.5 ms	95.32%
Experiment 1	Low Noise Mean	81.9 ms	166.3 ms	549.1 ms	833.0 ms	72.25%
	Medium Noise Mean	94.0 ms	193.0 ms	541.9 ms	821.3 ms	70.14%
	High Noise Mean	108.2 ms	244.5 ms	613.0 ms	896.8 ms	61.77%
Experiment 2	Low Noise Mean	100.1 ms	175.0 ms	545.3 ms	809.1 ms	90.07%
	Medium Noise Mean	93.6 ms	192.2 ms	565.3 ms	829.7 ms	89.59%
	High Noise Mean	94.5 ms	228.0 ms	629.9 ms	925.3 ms	80.72%

Table 1. Summary statistics for each data type used in this study across both EEG sessions and visual noise conditions for a total sample size of 147. Experiment 1 had a sample size of 63 (21 unique EEG sessions per visual noise condition). Experiment 2 had a sample size of 84 (28 unique EEG sessions per visual noise condition). N200 peak-latencies, 10th percentile reaction times, and median reaction times become longer in more difficult (lower accuracy) noise conditions. This is not true of N200 deflection times in experiment 2. VET is expected to become longer when segregation of the visual target is more difficult in conditions of high noise contrast.

measures are given in **Table 2**. It should be noted that four of the subjects were considered trained on the task, with two subjects completing 9 sessions (both experiments) and two other subjects completing 7 sessions of the second experiment.

Simple results: Scatter plots and linear regression

In order to explore the hypothesis that trial-averaged N200 peak-latency predicts session-level visual encoding time, linear models between reaction time percentiles (both correct and incorrect reaction times combined) and N200 peak-latencies were computed. In evidence accumulation models of quick decision making, the *shifts* of reaction time (RT) distributions (and thus the small RT percentiles) should correlate with NDT (i.e. VET + residual motor response time) while the shape of RT distributions (and thus the medium and larger RT percentiles) should correlate both with NDT *and* decision making properties. Thus linear regressions can be explored without fitting decision-making models to data directly. A close to 1-to-1 relationship was found between in a simple linear regression between trial-averaged N200 latencies and 10th RT percentiles as shown in the middle portion of **Figure 4** with a regression coefficient of $\beta_1 = 1.32$ ($N = 147$, 95% confidence interval: $[0.83, 1.81]$, $p < .001$, $t = 5.33$, $\log(\mathrm{BF}) = 10.44$, $\mathrm{BF1} = 7.40$). Although it should be noted that only 16% of the variance in 10th RT percentiles were explained by the variance across trial-averaged N200 latencies ($R^2_{adj} = .162$). This latter finding might be expected if other trial-invariant mechanisms besides visual encoding time (VET) contribute to the variance in NDT, such as residual motor response.

The relationship is also expected to be observed in the reaction time distributions itself, albeit with more variance around the regression line. Single-trial estimates of N200 latencies were compared to reaction times across all data points. Again, a close to 1-to-1 relationship was found between in a simple linear regression between single-trial N200 peak-latencies and reaction times as shown in the right portion of **Figure 4** with a regression coefficient of $\beta_1 = 0.95$ ($N = 13{,}426$, 95% confidence interval: $[0.84, 1.07]$, $p < .001$, $t = 15.85$, $\log(\mathrm{BF}) = 120.42$, $\mathrm{BF1} = 25.91$). However only about 2% of the variance of raw single-trial reaction times were explained ($R^2_{adj} = .018$). This is expected since other mechanisms besides visual encoding time (VET) should contribute to the variance in reaction times, which was explored with the following cognitive modeling results.

Data summary across unique subjects ($N = 14$)

	N200 Deflection times	N200 Peak-latencies	10th Percentile Reaction times	Median Reaction times	Mean Accuracy
Minimum	57.7 ms	183.2 ms	482.3 ms	649.1 ms	62.67%
Mean	91.7 ms	199.5 ms	567.3 ms	839.7 ms	72.33%
Maximum	129.2 ms	225.3 ms	676.2 ms	1070.8 ms	90.14%

Table 2. Summary statistics for each data type averaged within each of the 14 unique subjects. All measures varied widely across subjects suggesting individual differences in VET and other decision-related cognitive processes. Some of these individual differences account for the variation in N200 deflection times and N200 peak-latencies observed in the distributions presented in **Figure 3**. While not the focus of this particular study, future work should seek to discover if individual differences in VET are explained by individual differences in N200 peak-latencies (a hypothesis expected from the results of the research presented here).

No relationship was found between N200 deflection times across trials and 10th RT percentiles ($N = 147$, $p < .301$, $t = -1.04$, $\log(\text{BF}) = -1.24$, $\text{BF1} < .001$). The linear regression is shown in the left portion of **Figure 4**. In fact, the Bayes Factor BF1 displayed evidence strongly in favor of $\beta \neq 1$ ($1/\text{BF1} = 225.96$). This suggests that while N200 deflection times may reflect an early visual processing stage, variance across noise conditions and EEG sessions does not correspond with variance in reaction time distribution shifts across noise conditions and EEG sessions.

Cognitive model fitting results

Each model was fit using JAGS with six Markov Chain Monte Carlo (MCMC) chains run in parallel of 52,000 samples each with 2,000 burn-in samples and a thinning parameter of 10 resulting in 5,000 posterior samples in each chain. The posterior samples from each chain were combined to form one posterior sample of 30,000 samples for each parameter. Model convergence was evaluated based on the Gelman-Rubin statistic $\hat{R}$, which compares the estimated between-chains and within-chain variances for each model parameter (Gelman and Rubin, 1992). Using this statistic all three models were judged to have converged, with $\hat{R} \leq 1.03$ for all parameters in each model ($\hat{R} > 1.10$ for any parameter is usually deemed evidence for a lack of convergence of the entire model).

Model 1 was used to evaluate the effect of trial-averaged N200 peak-latency on NDT across EEG sessions and noise conditions. The mean effect across all conditions of each experiment μ_γ provides a sense of how N200 processing time tracks NDT in general. The posterior distribution of this parameter was found to be around 1 in each condition and experiment as shown in **Figure 5**, indicating that 1 ms increase in N200 processing corresponded to 1 ms increase in NDT. The posterior distribution of the overall hierarchical effect of N200 peak-latency on NDT across sessions is plotted at the top of **Figure 5**, indicating that the overall Bayes Factor for a 1-to-1 relationship between N1 latency and NDT is $\text{BF1} = 4.90$, indicating moderate evidence (median = 0.67, 95% credible interval: $[-0.13, 1.66]$). An undetermined effect of trial-averaged N200 peak-latency on evidence accumulation rate (median = -3.23 evidence units per second, 95% credible interval: $[-6.53, 0.16]$) was found. There may be a positive effect of trial-averaged N200 peak-latency on boundary separation (median = 1.59 evidence units per second, 95% credible interval: $[0.09, 3.06]$), assuming that boundary separation is well estimated.

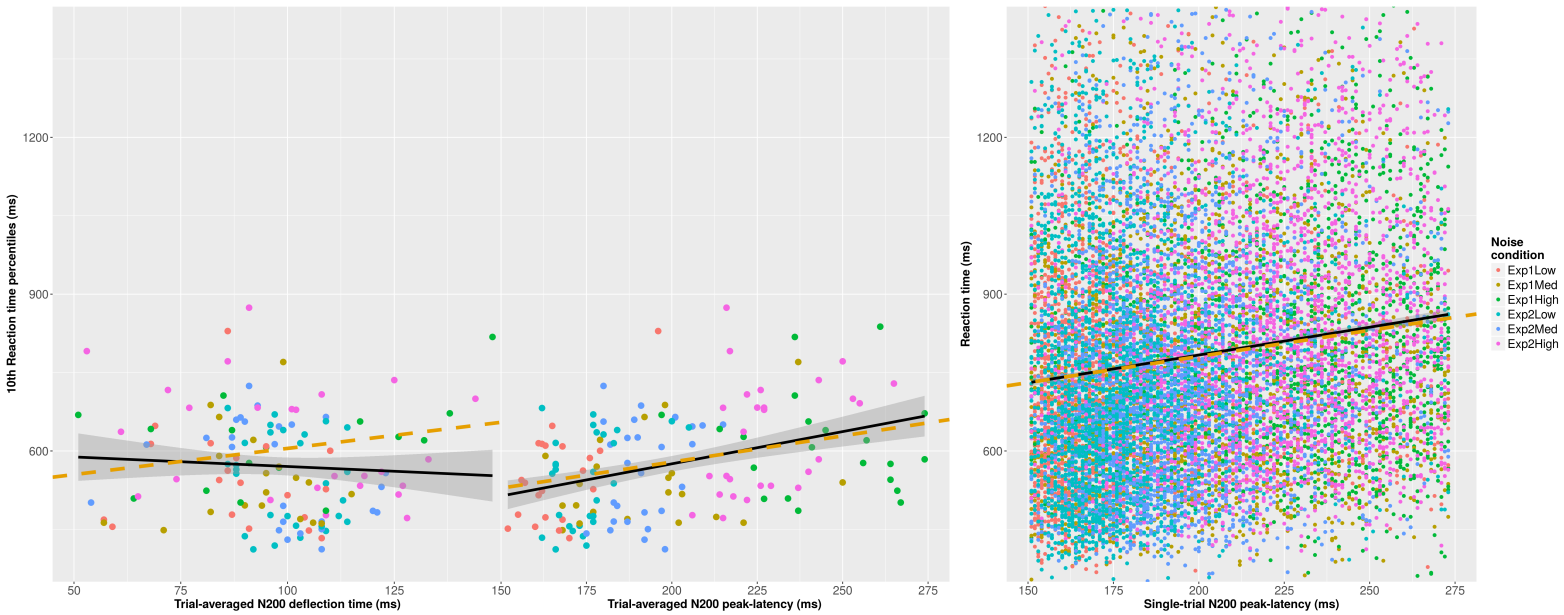

Figure 4. Left: A scatter plot of trial-averaged N200 deflection times and 10 reaction time percentiles (an estimate of the processing time of time-invariant cognition across trials) Middle: A scatter plot of trial-averaged N200 peak-latencies and 10th reaction time percentiles. Observations were generated per noise condition and per EEG collection session ($N = 147$). Right: A scatter plot of single-trial N200 latencies versus single-trial reaction times. Observations were generated per trial ($N = 13{,}426$). Best-fit simple linear regression lines are shown in black with 95% confidence intervals for the intercept and slope parameters shown in gray. Overlaid on the linear regression lines are gold dashed lines representing the hypothesis with a slope of 1. That is, the expected influence of N200 peak-latency on reaction time is 1-to-1 millisecond if N200 peak-latency reflected human visual encoding time (VET).

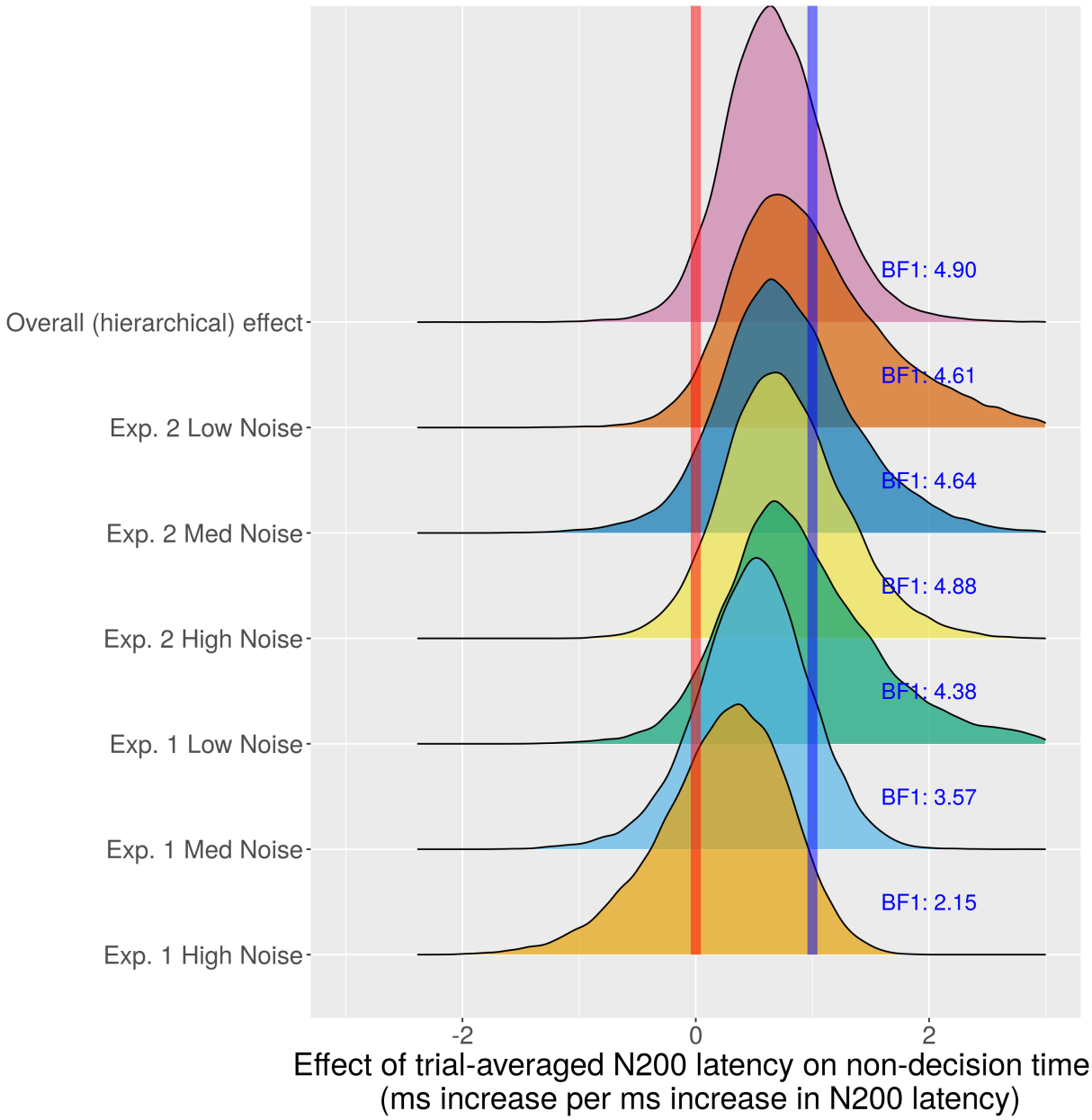

Figure 5. Posterior distributions of effects of N200 peak-latency on NDT (Model 1). Posterior distributions provide measures of parameter uncertainty in Bayesian model-fitting methods. If the posterior distributions had most of their density around the blue line, this would be strong evidence for the 1-to-1 relationship when the model assumptions are true. Posterior distributions centered on the red line would be strong evidence for the null hypothesis (the effect parameter equals 0). Observations were generated per noise condition and per EEG collection session, resulting in 147 observations used in the linear model of trial-averaged N200 peak-latency on NDT embedded in a hierarchical decision-diffusion model. Some evidence exists for the effects of N200 peak-latency on NDT to be 1-to-1 (one millisecond increase in N200 peak-latency corresponds to a millisecond increase in NDT) as indicated by the Bayes Factors calculated with a Savage-Dickey density ratio (Verdinelli and Wasserman, 1995) of the posterior density over the prior distribution at $\gamma = 1$.

Model 2 was fit post-hoc in order to evaluate the observed modifying effect of noise condition on effect of N200 peak-latency (see increasing trend across conditions in **Figure 5**). The results were inconclusive. Not much evidence was found for the null models as indicated by the Bayes Factors near 1 for the null effects $BF0$ as shown in **Figure 6**. However, not much evidence exists for *the existence* of moderator effects θ either. The base effect posterior distribution (evidence for the effect of N200 peak-latency on NDT in Experiment 1 in the low noise condition) was close to that of the overall effect posterior in Model 1 (BF1 = 4.46, median = 1.18, 95% credible interval: $[-0.12, 2.54]$). Undetermined effects of trial-averaged N200 peak-latency on evidence accumulation rate (median = -2.85 evidence units per second, 95% credible interval: $[-6.34, 0.71]$) and boundary separation (median = 1.28 evidence units per second, 95% credible interval: $[-0.74, 3.46]$) were found that were not differentiable from no effects.

Model 3 was fit in order to evaluate the effect of single-trial N200 peak-latency on non-decision for each EEG. In Model 3, the hierarchical effect parameter μ_γ provides a sense of how *single-trial* N200 peak-latency effects NDT. This parameter suggested that the overall single-trial effect was positive (median = 0.23, 95% credible interval: $[0.02, 0.44]$), but no evidence was found that this single-trial effect was equal to 1 (BF1 $<$ .001; reflecting that there was *not* a 1-to-1 correspondence on single-trials between N200 peak-latency and NDT). This result is to be expected with the presence of unremoved contaminant trials (see section below). Undetermined effects of single-trial N200 peak-latency on evidence accumulation rate (median = -0.40 evidence units per second, 95% credible interval: $[-1.72, 0.97]$) and boundary separation (median = 0.25 evidence units per second, 95% credible interval: $[-0.24, 0.78]$) were found that were not differentiable from no effect.

Simulations with contaminant trials

The simulations presented in the Methods section also reveled that the model can still recover some true NDTs on the EEG session level with the presence of "contaminant" trials. That is, some trials were expected to be from processes other than decision-making (i.e. "contaminant processes" for cognitive model fitting). These "mind-wandering" processes were simulated such that the amount of trials with processes unrelated to decision-making (e.g. see Hawkins et al., 2015) was systematically varied. The ability to recover accurate estimates of NDTs from 10th percentiles and

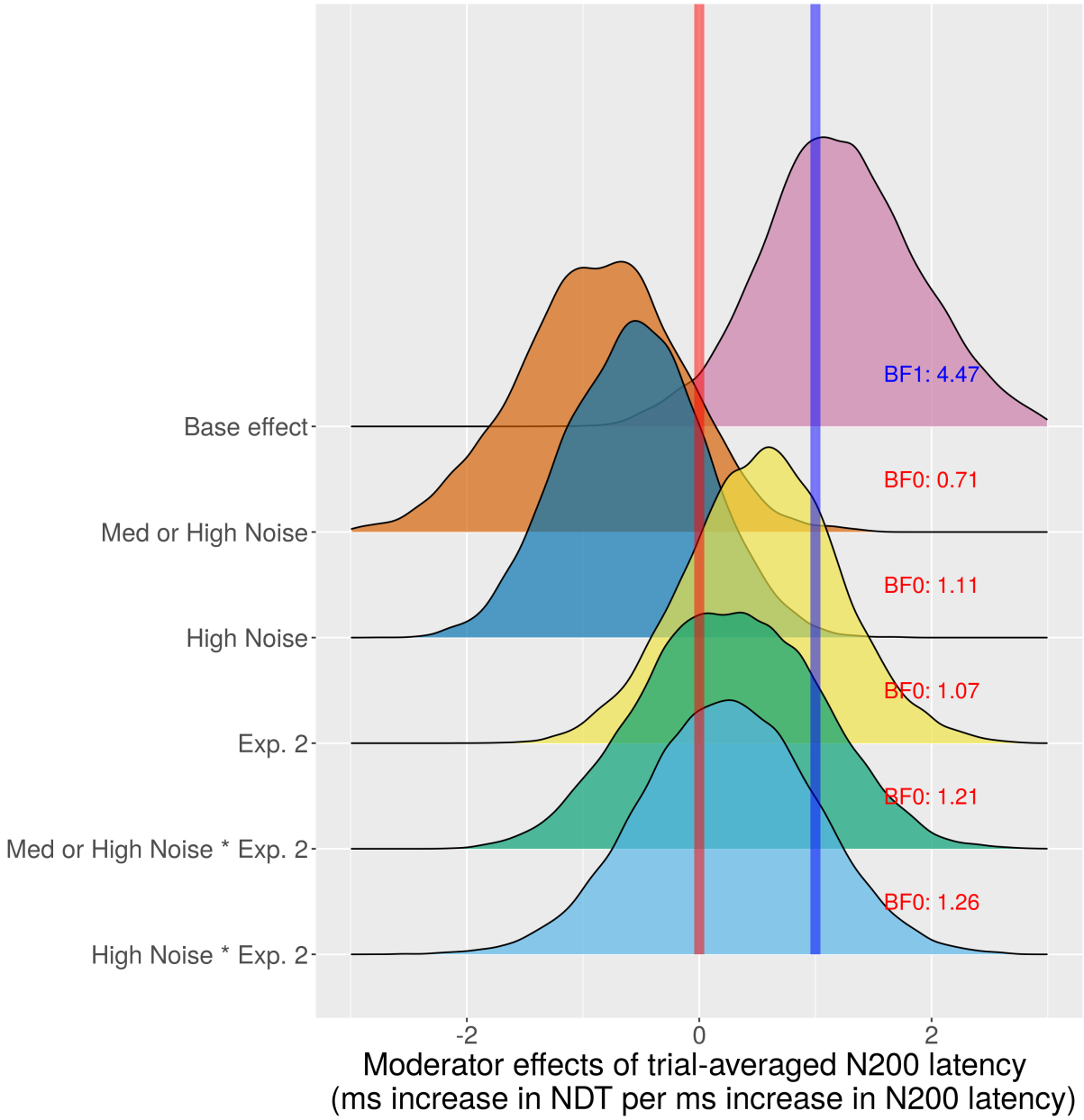

Figure 6. Session-level moderator effects (posterior distributions) of N200 peak-latency on NDT during the training experiment (Model 2). Observations were generated per noise condition and per EEG collection session, resulting in 147 observations used in the linear model of trial-averaged N200 peak-latency on NDT embedded in a hierarchical decision-diffusion model. The tests for moderator effects were inconclusive. Not much evidence exists for moderator effects of condition. There is also not much evidence for *no* moderator effects as indicated by the Bayes Factors for the null effects BF near 1 (e.g. there is not much evidence for $\theta = 0$, no effect of condition on the N200 and NDT relationship)

the hierarchical Bayesian fitting procedure with JAGS (Plummer, 2003; Wabersich and Vandekerckhove, 2014) was assessed. Also assessed was the regression slope between true NDT and estimated NDT. It was hypothesized that the regression slope between true NDT and estimated NDT would be less in trials with more contaminant processes that were not removed from the 350 millisecond cutoff (e.g. to remove fast errors). This was a post-hoc hypothesis that evaluated the reasons for a slope less than 1 in high noise contrast trials between trial-averaged N200 peak-latency and estimated NDT (see **Figure 5**).

The results suggested that more mind-wandering leads to slope parameters less than 1 in conditions with the presence of more contaminant trials but that 10th percentiles reflect the true relationship the trend of true NDT across subjects (although they overestimate NDTs by approximately 60 ms), and therefore would be more immune to contaminant processes. Therefore if N200 peak-latency reflected a true additive NDT process (i.e. visual encoding time; VET) this would explain the presence of a 1-to-1 relationship in the linear regressions of N200 peak-latency and 10th RT percentiles (**Figure 4**) but a lack of 1-to-1 relationship between N200 peak-latency and estimated NDTs when fitting decision-diffusion models directly (**Figure 5**). It should be noted that VET is only one theorized process of estimated NDT, but that the addition of uncorrelated non-decision cognitive processes to NDT would not affect linear regressions between VET and true NDT besides additional uncorrelated noise.

Source localization of N200 peaks

Cortical topographic maps were generated by projected spline-Laplacians onto one subject's cortical surface (method described above). Cortical topographic maps of this average peak across EEG sessions and noise conditions are given in **Figure 8**. The source estimation method described above suggested that N200 peaks in this study could be found in the following extrastriate cortical locations (such that the locations listed here were present in at least 60% of the localizations across EEG sessions and noise conditions): the angular gyri (both left and right hemispheres), the supramarginal gyri (both hemispheres), the superior parietal gyri (both hemispheres), the middle temporal gyri (both hemispheres), the postcentral gyri (both hemispheres), the left postcentral sulcus, and the left precentral gyrus. It should be noted that only the superior parietal gyri and the angular gyri overlap with those areas found by Nunez et al.

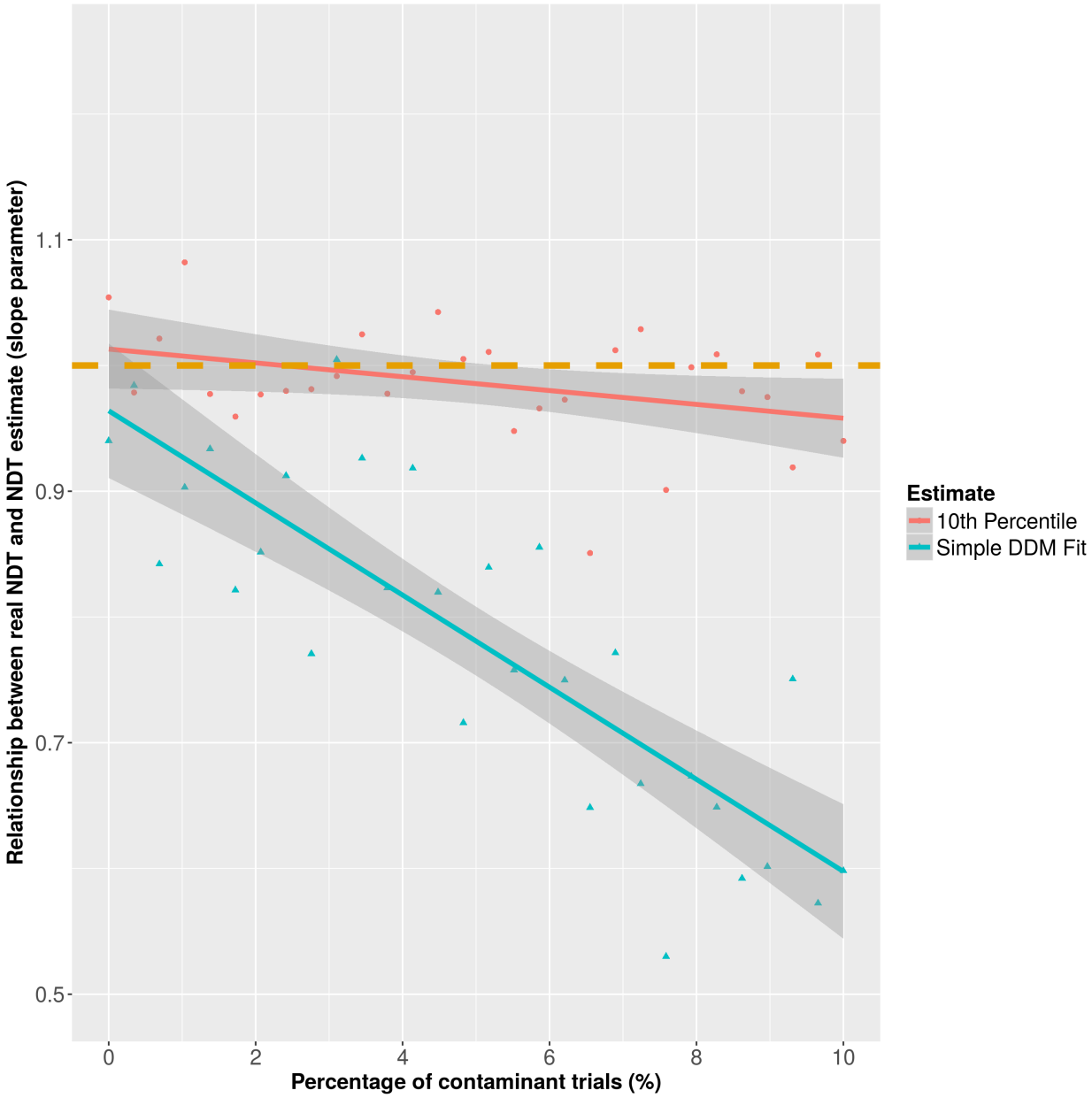

Figure 7. The addition of more trials with a contaminant (e.g. "mind-wandering") processes resulted in some non-decision time (NDT) estimates being negatively biased towards smaller values. This, in turn, resulted in decreased linear relationships (e.g. less than 1-to-1) between true NDT and estimated NDT. This was especially true for the hierarchical Bayesian estimates of simple decision-diffusion (DDM) model parameters, while the slopes between true NDT and 10th percentiles did not change much from 1-to-1 when more trials were added with a contaminant process. This suggested that while 10th percentiles were positively biased as estimates of true NDT (e.g. true NDT were approximately 60 milliseconds shorter than the 10th percentiles), the 1-to-1 relationship could be well estimated by the 10th percentiles but not the DDM fitting procedure when there were greater than 1% of trials with an unremoved contaminant process. This fact explains why a true measure of VET, such as the proposed N200 peak-latency, might not track DDM-estimated NDT well but would track 10th percentiles well.

(2017). This may be due to different loci of visual processing in the two studies or due to localization errors in either study.

Two interesting finds are suggested by the localization process. One is that the N200 waveforms are distributed across the cortex and not localized to one particular area. This may be reflective of the network that gives rise to the N200 peaks instead of local processing. This network activity is expected by a global model of event-related EEG (Nunez and Srinivasan, 2014). The second interesting finding is that the N200 peaks are localized more to one side in almost every subject, but not the same side across subjects (although the right side of the extrastriate is present in most localizations). This suggests that visual encoding of the central stimulus may involve a dominate lateralized visual network, because the subjects are favoring a particular visual field (left or right).

Work by Mishkin et al. (1983) and Lamme and Roelfsema (2000), among others, suggest that the segregation of the target Gabor from visual noise would occur in the temporal "segregation" pathway of the primate cortex at about 150 milliseconds (after a delay due to feedforward and feedback visual network behavior). The localization in human extrastriate and temporal locations points to the N200 peak-latency being the time point at which the target Gabor is "segregated" from visual noise in the human cortex, in order to accumulate visual evidence for a motor response. This is further evidence that the N200 peak-latency represents VET, the time before evidence accumulation, along with the 1-to-1 evidence that N200 peak-latencies track NDT previously discussed.

Discussion

Evidence is presented both for and against the N200-VET hypothesis. Evidence against hypotheses are often left out of manuscripts presented in exploratory analyses in both the cognitive psychology and cognitive neuroscience fields, often presented as confirmatory results. Such "censoring" of data can lead to biased statistical analyses (Sterling, 1959; Rosenthal, 1979; Guan and Vandekerckhove, 2016).

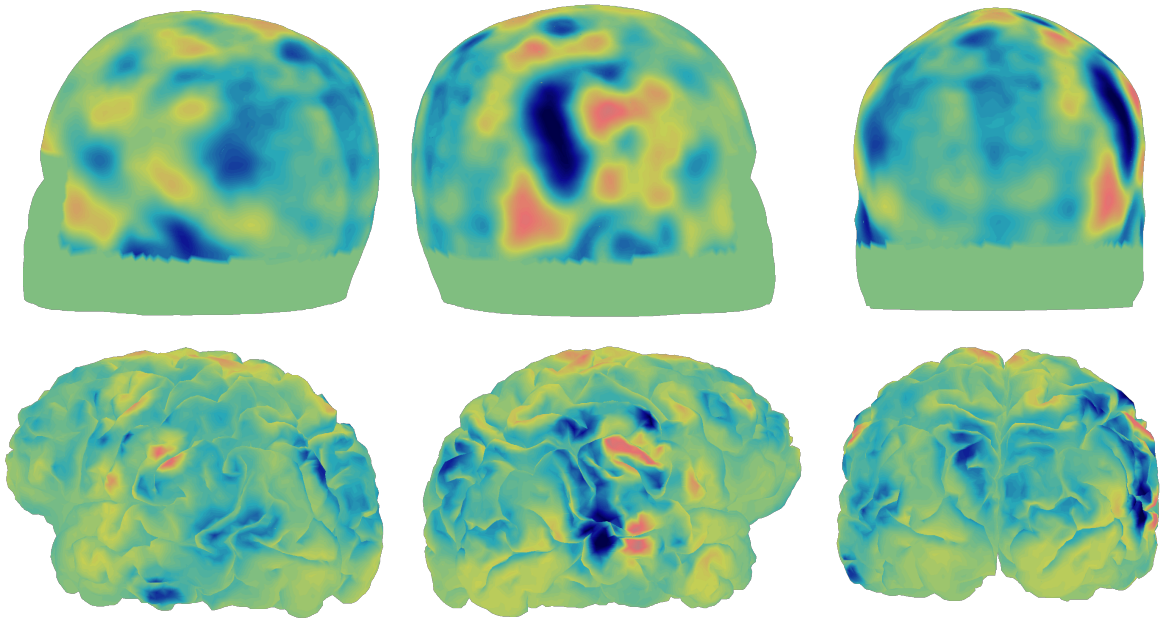

Figure 8. Right and left sagittal and posterior views of localized trial-averaged N200 waveforms averaged across all EEG recordings and conditions ($N = 147$). Current Source Density MNI scalp topographies (Top) were generated with a Laplacian transform of EEG data (a projection of the first SVD component) with spline-interpolation between electrodes (Nunez and Pilgreen, 1991; Deng et al., 2012; Kayser and Tenke, 2015) . The cortical maps (Bottom) were obtained by projecting the MNI-scalp spline-Laplacians onto one subject's anatomical fMRI image via Tikhonov (L2) regularization, maintaining similar distributions of activity of the surface Laplacians on the cortical surface. Blue and orange regions correspond to cortical areas estimated to produce negative and positive potentials observed on the scalp respectively. This localization suggests N200 activity occurs as a result of segregation of the target from visual noise due to the parietal and temporal locations suggesting activation of the "segregation pathway" (Mishkin et al., 1983; Lamme and Roelfsema, 2000). However variance in assumptions necessary for EEG localization across algorithms would yield diverse conclusions about the localization of this N200 activity (Nunez and Srinivasan, 2006).

Evidence FOR N200 peak-latencies tracking visual encoding time

Both simple regression analyses yielded evidence for a relationship between EEG measures of neural processing speed (N200 waveforms) and visual encoding times (VET). These regression fits indicate that there was 1) approximately a 1 ms increase in reaction times when there was a 1 ms increase in single-trial N200 peak-latency and 2) approximately a 1 ms increase in the 10th percentile of reaction times, a non-parametric estimate of NDT, when there was a 1 ms increase in trial-averaged N200 peak-latencies across both experiments and all experimental sessions and all visual noise conditions of EEG. Furthermore, moderate evidence was found of this 1-to-1 relationship of both single-trial N200 latencies and trial-average N200 peak-latency on NDT in hierarchical decision-diffusion Models 1 and 2.

These findings match previous research. In particular, Stanford et al. (2010) show that the accuracies of monkeys when evidence accumulation is impossible for 200 ms after target onset are near chance while accuracies when evidence accumulation is impossible for only 100 ms after target onset are more reflective of a completed decision, suggesting that visual encoding time must take somewhere between 100 ms and 200 ms for the simple color discrimination task. N200 peak-latencies reflecting visual encoding time would also explain why N200 latencies have been found to engage bottom-up, top-down attention, and a visual attention discriminating process (Vogel and Luck, 2000). In this study we found significant noise-condition effects in N200 peak-latency (see **Table 1**) such that N200 peak-latencies become longer with larger amounts of visual noise contrast (this finding was not observed in the N200 deflection times), and it is expected the VET should become longer with larger amounts of visual noise due to a higher cognitive difficulty of target-noise segregation. Furthermore we found significant individual differences in N200 peak-latencies across subjects, which matches expectations that individual differences in cognitive processing exists that explains individual differences in behavior (e.g. Schubert et al., 2017). Finally our findings in this study closely match findings discussed by Thorpe et al. (1996); Martin et al. (2010); Zhang et al. (2016); Loughnane et al. (2016) as discussed in the Introduction of this paper.

Evidence AGAINST N200 peak-latencies tracking visual encoding time

When exploring the relationship between N200 peak-latencies and NDT directly in DDM, the ability of ERP latencies to reflect visual encoding time seems to depend upon the quality of visual stimuli. In two experiments with different noise types, the effects of N200 peak-latency differences on NDT differences (assumed to be the sum of VET and residual motor response time) across EEG sessions seemed to be mediated by the contrast condition of the visual distractors. This suggests that how well the peak neural signal latency tracks visual encoding time is dependent upon the quality of the external signal itself. However, not much evidence was found for this qualitative finding as indicated by the Bayes Factors of the null model in **Figure 6**.

It may also suggest there is a larger presence of "contaminant" reaction times in high noise conditions that effect estimates of NDT (such as trials when the subject is not focused on the task–dubbed "mind-wandering" by the Cognitive Neuroscience field) Hawkins et al., 2015; Fox et al., 2015). Simulation revealed that NDTs were not as well estimated when more mind-wandering trials were introduced. And that the 1-to-1 relationship between true visual encoding times and NDTs were not as robust. This was due to the presence of negatively biased estimates of NDT when more contaminant trials occurred. That is, true NDT was larger than was estimated for some subjects, this in turn decreased the slope of the relationship between true NDT and NDT estimates (see **Figure 7**. This explains the weaker relationships between N200 peak-latency and NDT, such that N200 peak-latency could be a good biomarker of VET and that NDTs are not well estimated high noise contrast (e.g. more difficult) conditions. However, while the 10th percentile estimates of NDT were biased, they were not as influenced by the addition of mind-wandering process. This explains why the relationship between N200 latencies and 10th percentile estimates remained 1-to-1 in more difficult experimental conditions. Evidence has previously been found that larger amounts of mind-wandering (and thus contaminant trials) can occur in more difficult task conditions (Feng et al., 2013).

Single-trial N200 latencies may not be related to NDT in high noise conditions. However, further work is required to find better, testable estimates of single-trial neural processing speed as measured by ongoing EEG. It is also possible that the simple decision-diffusion model does not provide a satisfactory account of visual encoding with the presence of contaminant processes, as suggested by the near 1-to-1 relationship between single-trial N200 peak-latencies and

reaction times on single trials (see **Figure 4**. Better theoretical models of behavior with trial-to-trial variability in NDT may be needed, such as cognitive models that include both decision processes and mind-wandering processes (e.g. see van Vugt et al., 2015; Mittner et al., 2016).

A neurocognitive theory of quick decision making

A neurocognitive model of encoding, evidence accumulation, and motor response is proposed that is identified with separable measures of VET and motor response that are estimated from observed EEG, accuracy, and reaction time distributions. Fitting this type of model to data would allow direct hypothesis testing of observed trial-to-trial differences and individual differences in neural signals as well as human behavior during quick decision making.

Neurocognitive hierarchical models of VET, evidence accumulation, and motor response time become identifiable when treating EEG measures (e.g. N200 peak-latencies) as measures of VET. The theory is an extension of a class of Decision-Diffusion Models (e.g. "drift-diffusion" models, see Ratcliff and McKoon, 2008, for a review) which predicts that reaction time and accuracy are explained by a continuous accumulation of evidence towards certain pre-decided evidence thresholds (see **Figure 9**).

A decision-diffusion model of accuracy ($w = 0$ or $w = 1$) and reaction time t on one trial is predicted to be a function of VET τ_e, motor response time τ_m, the drift rate which is the average rate of evidence accumulation within one trial δ, the diffusion coefficient ς which is the variance around the average rate of evidence accumulation within a trial, and the amount of evidence required to make a decision α_t, which may be assumed to decrease with time. The bias towards correct or incorrect responses is assumed to be equal to $z_0 = 0.5\alpha_t$. The joint density f of RT t and accuracy w of this simplified diffusion model is given in **Equation 1**. The density is derived from the solution given by (Ratcliff, 1978; Tuerlinckx, 2004).

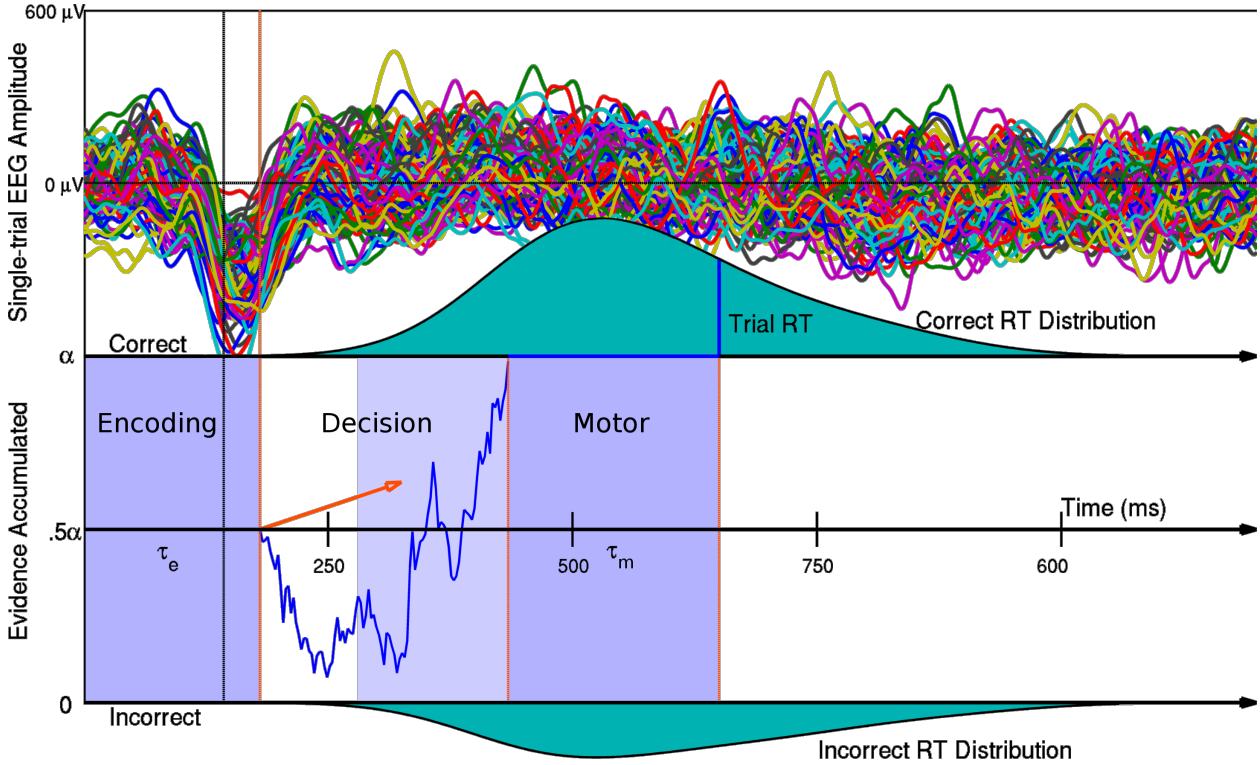

Figure 9. A graphical illustration of a Neural Decision Diffusion model in which the encoding time τ_e on single-trials describes the latency of the negative peaks of the N200 waveform on 146 experimental trials. Single-trial observations of the N200 peak-latency are found by using a decomposition of the average ERP response at each electrode and then biasing the raw EEG by the resulting channel weights. Total NDT τ reflects both visual encoding time (VET) τ_e as well as residual motor response τ_m (i.e. motor preparation time after the decision is made) and can be estimated from reaction time distributions. Decision time is generated via a Brownian motion evidence accumulation process with evidence accumulation rate δ (drift rate), evidence accumulation noise ς (diffusion coefficient), and evidence threshold (boundary parameter) α (for more information see Ratcliff, 1978; Ratcliff and McKoon, 2008; Nunez et al., 2015, 2017)

$$
\begin{cases}
f(t, w=0 \mid \alpha, \varsigma^2, \tau_e, \tau_m, \delta) = \frac{\pi\varsigma^2}{\alpha_t^2} e^{-\frac{1}{2\varsigma^2}\left[\delta\alpha_t + \delta^2(t-\tau_e-\tau_m)\right]} \sum_{k=1}^{\infty} \left[k \sin\left(\frac{1}{2}\pi k\right) e^{-\frac{1}{2\alpha_t^2} k^2 \pi^2 \varsigma^2 (t-\tau_e-\tau_m)} \right] \\
\\
f(t, w=1 \mid \alpha, \varsigma^2, \tau_e, \tau_m, \delta) = f(t, w=0 \mid \alpha, \varsigma^2, \tau_e, \tau_m, -\delta)
\end{cases}
\tag{1}
$$

Note that the density in **Equation 1** is classically unidentifiable when estimating the model with only reaction time and accuracy observations for two reasons. 1) Encoding time τ_e and motor response time τ_m both contribute to residual response time $\tau = \tau_e + \tau_m$ which approximately equals the smallest observed reaction times that are not due to contaminant trials. 2) Only two of the three parameters related to evidence accumulation (i.e. drift rate δ, the diffusion coefficient ς, and the boundary separation α) can be found with behavioral data alone. For example, if α_t is constant with t, multiplying ς by two and dividing both α and δ by two would result in the same fit of choice-RT (Wabersich and Vandekerckhove, 2014).

Fitting cognitive neuroscientific results to cognitive models is a growing field of research (Mulder et al., 2014; Turner et al., 2015; de Hollander et al., 2016; Turner et al., 2017). The goal of future work is to further develop theory that reconciles psychological phenomena with observations about the human brain found in the cognitive neuroscience literature. This work would lead to the ability to fit the density given in **Equation 1** with *identifiable* parameters that explain both psychological phenomena and observed brain electrophysiology. This would allow researchers to fit the full model to data and give researchers the ability to directly test hypotheses about the cognitive and computational reasons behind observed human brain behavior in both healthy and clinical populations.

References

de Hollander G, Forstmann BU, Brown SD (2016) Different ways of linking behavioral and neural data via computational cognitive models. *Biological Psychiatry: Cognitive Neuroscience and Neuroimaging* 1:101–109.

Deng S, Winter W, Thorpe S, Srinivasan R (2012) Improved surface laplacian estimates of cortical potential using realistic models of head geometry. *IEEE Transactions on Biomedical Engineering* 59:2979–2985.

Desimone R, Duncan J (1995) Neural mechanisms of selective visual attention. *Annual Review of Neuroscience* 18:193–222.

Dickey JM, Lientz BP et al. (1970) The weighted likelihood ratio, sharp hypotheses about chances, the order of a markov chain. *The Annals of Mathematical Statistics* 41:214–226.

Dmochowski JP, Norcia AM (2015) Cortical components of reaction-time during perceptual decisions in humans. *PloS one* 10:e0143339.

Feng S, D'Mello S, Graesser AC (2013) Mind wandering while reading easy and difficult texts. *Psychonomic Bulletin & Review* 20:586–592.

Fischl B, van der Kouwe A, Destrieux C, Halgren E, Ségonne F, Salat DH, Busa E, Seidman LJ, Goldstein J, Kennedy D et al. (2004) Automatically parcellating the human cerebral cortex. *Cerebral Cortex* 14:11–22.

Fox KCR, Spreng RN, Ellamil M, Andrews-Hanna JR, Christoff K (2015) The wandering brain: Meta-analysis of functional neuroimaging studies of mind-wandering and related spontaneous thought processes. *Neuroimage* 111:611–621.

Gelman A, Rubin DB (1992) Inference from iterative simulation using multiple sequences. *Statistical Science* pp. 457–472.

Gold JI, Shadlen MN (2007) The neural basis of decision making. *Annual Review of Neuroscience* 30:535–574.

Guan M, Vandekerckhove J (2016) A bayesian approach to mitigation of publication bias. *Psychonomic Bulletin & Review* 23:74–86.

Hawkins GE, Mittner M, Boekel W, Heathcote A, Forstmann BU (2015) Toward a model-based cognitive neuroscience of mind wandering. *Neuroscience* 310:290–305.

Hawkins GE, Mittner M, Forstmann BU, Heathcote A (2017) On the efficiency of neurally-informed cognitive models to identify latent cognitive states. *Journal of Mathematical Psychology* 76:142–155.

JASP Team T (2017) JASP (Version 0.8.1.2)[Computer software].

Jeffreys H (1961) *Theory of probability* Oxford University Press.

Kass RE, Raftery AE (1995) Bayes factors. *Journal of the American Statistical Association* 90:773–795.

Kayser J, Tenke CE (2003) Optimizing PCA methodology for ERP component identification and measurement: theoretical rationale and empirical evaluation. *Clinical Neurophysiology* 114:2307–2325.

Kayser J, Tenke CE (2015) Issues and considerations for using the scalp surface Laplacian in EEG/ERP research: A tutorial review. *International Journal of Psychophysiology* 97:189–209.

Lamme VAF, Roelfsema PR (2000) The distinct modes of vision offered by feedforward and recurrent processing. *Trends in neurosciences* 23:571–579.

Lee MD (2008) Three case studies in the Bayesian analysis of cognitive models. *Psychonomic Bulletin & Review* 15:1–15.

Lee MD, Newell BJ (2011) Using hierarchical Bayesian methods to examine the tools of decision-making. *Judgment & Decision Making* 6.

Lin CT, Chuang CH, Kerick S, Mullen T, Jung TP, Ko LW, Chen SA, King JT, McDowell K (2016) Mind-wandering tends to occur under low perceptual demands during driving. *Scientific Reports* 6.

Loughnane GM, Newman DP, Bellgrove MA, Lalor EC, Kelly SP, O'Connell RG (2016) Target selection signals influence perceptual decisions by modulating the onset and rate of evidence accumulation. *Current Biology* 26:496–502.

Luck SJ (2012) Event-related potentials In Cooper H, Camic PM, Long DL, Panter AT, Rindskopf D, Sher KJ, editors, *APA Handbook of Research Methods in Psychology: Volume 1, Foundations, Planning, Measures, and Psychometrics*. American Psychological Association.

Makeig S, Bell AJ, Jung TP, Sejnowski TJ (1996) Independent component analysis of electroencephalographic data. *Advances in Neural Information Processing Systems* 8:145–151.

Martin T, Huxlin KR, Kavcic V (2010) Motion-onset visual evoked potentials predict performance during a global direction discrimination task. *Neuropsychologia* 48:3563–3572.

Miąsko T (2017) pyjags 1.2.2 `https://github.com/tmiasko/pyjags`.

Mishkin M, Ungerleider LG, Macko KA (1983) Object vision and spatial vision: two cortical pathways. *Trends in neurosciences* 6:414–417.

Mittner M, Hawkins GE, Boekel W, Forstmann BU (2016) A neural model of mind wandering. *Trends in cognitive sciences* 20:570–578.

Mulder MJ, van Maanen L, Forstmann BU (2014) Perceptual decision neurosciences – a model-based review. *Neuroscience* 277:872–884.

Neyman J, Pearson ES (1933) On the problem of the most efficient tests of statistical hypotheses. *Philosophical Transactions of the Royal Society of London. Series A, Containing Papers of a Mathematical or Physical Character* 231:289–337.

Nunez MD (2017) Refining understanding of human decision making by testing integrated neurocognitive models of EEG, choice and reaction time Ph.D. diss., University of California, Irvine.

Nunez MD, Nunez PL, Srinivasan R (2016) Electroencephalography (EEG): neurophysics, experimental methods, and signal processing In Ombao H, Linquist M, Thompson W, Aston J, editors, *Handbook of Neuroimaging Data Analysis*, pp. 175–197. Chapman & Hall/CRC.

Nunez MD, Srinivasan R, Vandekerckhove J (2015) Individual differences in attention influence perceptual decision making. *Frontiers in Psychology* 6:18.

Nunez MD, Vandekerckhove J, Srinivasan R (2017) How attention influences perceptual decision making: Single-trial EEG correlates of drift-diffusion model parameters. *Journal of Mathematical Psychology* 76, Part B:117–130.

Nunez PL, Pilgreen KL (1991) The spline-laplacian in clinical neurophysiology: a method to improve EEG spatial resolution. *Journal of Clinical Neurophysiology* 8:397–413.

Nunez PL, Silberstein RB, Cadusch PJ, Wijesinghe RS, Westdorp AF, Srinivasan R (1994) A theoretical and experimental study of high resolution EEG based on surface laplacians and cortical imaging. *Electroencephalography and Clinical Neurophysiology* 90:40–57.

Nunez PL, Srinivasan R (2006) *Electric Fields of the Brain: The Neurophysics of EEG* Oxford University Press.

Nunez PL, Srinivasan R (2014) Neocortical dynamics due to axon propagation delays in cortico-cortical fibers: EEG traveling and standing waves with implications for top-down influences on local networks and white matter disease 1542:138–166.

O'Connell RG, Dockree PM, Kelly SP (2012) A supramodal accumulation-to-bound signal that determines perceptual decisions in humans. *Nature Neuroscience* 15:1729–1735.

Parra LC, Spence CD, Gerson AD, Sajda P (2005) Recipes for the linear analysis of EEG. *Neuroimage* 28:326–341.

Philiastides MG, Heekeren HR, Sajda P (2014) Human scalp potentials reflect a mixture of decision-related signals during perceptual choices. *The Journal of Neuroscience* 34:16877–16889.

Plummer M (2003) JAGS: A program for analysis of Bayesian graphical models using Gibbs sampling In *Proceedings of the 3rd International Workshop on Distributed Statistical Computing (DSC 2003), Vienna, Austria.*

Pommier J, Renard Y (2005) Getfem++, an open source generic c++ library for finite element methods.

Ratcliff R (1978) A theory of memory retrieval. *Psychological Review* 85:59.

Ratcliff R, McKoon G (2008) The diffusion decision model: theory and data for two-choice decision tasks. *Neural Computation* 20:873–922.

Rosenthal R (1979) The file drawer problem and tolerance for null results. *Psychological bulletin* 86:638.

Rouder JN, Morey RD (2012) Default bayes factors for model selection in regression. *Multivariate Behavioral Research* 47:877–903.

Schmolesky MT, Wang Y, Hanes DP, Thompson KG, Leutgeb S, Schall JD, Leventhal AG (1998) Signal timing across the macaque visual system. *Journal of neurophysiology* 79:3272–3278.

Schubert AL, Hagemann D, Frischkorn G (2017) Is intelligence little more than the speed of higher-order processing? *Journal of Experimental Psychology: General* .

Servant M, White C, Montagnini A, Burle B (2015) Using Covert Response Activation to Test Latent Assumptions of Formal Decision-Making Models in Humans. *Journal of Neuroscience* 35:10371–10385.

Servant M, White C, Montagnini A, Burle B (2016) Linking theoretical decision-making mechanisms in the simon task with electrophysiological data: A model-based neuroscience study in humans. *Journal of Cognitive Neuroscience* 28:1501–1521.

Shadlen MN, Kiani R (2013) Decision making as a window on cognition. *Neuron* 80:791–806.

Stanford TR, Shankar S, Massoglia DP, Costello MG, Salinas E (2010) Perceptual decision making in less than 30 milliseconds. *Nature neuroscience* 13:379–385.

Sterling TD (1959) Publication decisions and their possible effects on inferences drawn from tests of significance—or vice versa. *Journal of the American statistical association* 54:30–34.

Thorpe S, Fize D, Marlot C (1996) Speed of processing in the human visual system. *Nature* 381:520.

Tuerlinckx F (2004) The efficient computation of the cumulative distribution and probability density functions in the diffusion model. *Behavior Research Methods, Instruments, & Computers* 36:702–716.

Turner BM, Forstmann BU, Love BC, Palmeri TJ, Van Maanen L (2017) Approaches to analysis in model-based cognitive neuroscience. *Journal of Mathematical Psychology* 76:65–79.

Turner BM, van Maanen L, Forstmann BU (2015) Informing cognitive abstractions through neuroimaging: The neural drift diffusion model. *Psychological Review* 122:312–336.

van Vugt MK, Taatgen NA, Sackur J, Bastian M (2015) Modeling mind-wandering: a tool to better understand distraction In *Proceedings of the 13th International Conference on Cognitive Modeling*, pp. 252–257. University of Groningen.

Vandekerckhove J, Tuerlinckx F (2008) Diffusion model analysis with MATLAB: A DMAT primer. *Behavior Research Methods* 40:61–72.

Vandekerckhove J, Tuerlinckx F, Lee MD (2011) Hierarchical diffusion models for two-choice response times. *Psychological Methods* 16:44.

Verdinelli I, Wasserman L (1995) Computing Bayes factors using a generalization of the savage-dickey density ratio. *Journal of the American Statistical Association* 90:614–618 00422.

Vogel EK, Luck SJ (2000) The visual N1 component as an index of a discrimination process. *Psychophysiology* 37:190–203.

Voss A, Rothermund K, Voss J (2004) Interpreting the parameters of the diffusion model: An empirical validation. *Memory & Cognition* 32:1206–1220.

Wabersich D, Vandekerckhove J (2014) Extending JAGS: A tutorial on adding custom distributions to JAGS (with a diffusion model example). *Behavior Research Methods* 46:15–28.

Wagenmakers EJ (2009) Methodological and empirical developments for the ratcliff diffusion model of response times and accuracy. *European Journal of Cognitive Psychology* 21:641–671.

Wagenmakers EJ, Lodewyckx T, Kuriyal H, Grasman R (2010) Bayesian hypothesis testing for psychologists: A tutorial on the savage–dickey method. *Cognitive psychology* 60:158–189.

Webster MA, De Valois RL et al. (1985) Relationship between spatial-frequency and orientation tuning of striate-cortex cells. *JOSA A* 2:1124–1132.

Zhang Q, Walsh MM, Anderson JR (2016) The effects of probe similarity on retrieval and comparison processes in associative recognition. *Journal of Cognitive Neuroscience* .

Figure Legends

Figure 1 Example stimuli of the *cue* and *response* intervals of medium noise conditions from Experiments 1 (top) and 2 (bottom). During the response interval, subjects decided which spatial frequency each target Gabor matched, pressing a button with their left hand for a low spatial frequency target (2.4 cycles per degree visual angle, cpd) and pressing a button with their right hand for a high spatial frequency target (2.6 cpd). N200 waveforms were calculated time-locked to the onset of the Gabor stimulus during the response intervals. In both experiments a paradigm was used in which the visual noise changed at 40 Hz and the Gabor signal flickered at 30 Hz to evoke 40 Hz and 30 Hz responses in electrocortical activity that track attention to the noise and signal stimuli. While the attention analysis is not discussed in this paper, a similar analysis is presented by Nunez et al. (2015).

Figure 2 A visual representation of the singular value decomposition (SVD) method for finding single-trial estimates of evoked responses in EEG. The EEG presented here is time-locked to the signal onset during the response interval, such that the single-trial N200 waveform encoded the response to the signal onset. A single trial of EEG from one subject (Left) can be thought of as a time by channel ($T \times C$) matrix. The first SVD component explained the most variability in this subject's ERP response to the signal across all trials in the training set. SVD weights $\mathbf{v}$ ($C \times 1$) are obtained from the ERP response (i.e. trial-averaged EEG; $T \times C$) and can be plotted on a cartoon representation of the human scalp with intermediate interpolated values (Middle). This specific trial's N200 waveform (Right) was obtained by multiplying the time series data from each channel on this trial by the associated weight in vector $\mathbf{v}$ and then summing across all weighted channels. Weight averaging across channels is a common method to obtain larger signal-to-noise ratios in EEG (e.g. cleaner, more task-relevant neural signals, see Parra et al., 2005).

Figure 3 All trial-averaged N200 waveforms across EEG sessions and the 3 visual noise experimental conditions ($N = 147$). Smoothed histograms for the N200 deflection times (green distribution) as well as the N200 peak-latency times (blue distribution) are also displayed above. There was a significant but weak correlation found between the found N200 deflection times and the N200 peak-latency times ($\rho = .274$). N200 deflection times are not as variable across EEG sessions and noise conditions as N200 peak-latencies.

Figure 4 Left: A scatter plot of trial-averaged N200 deflection times and 10 reaction time percentiles (an estimate of the processing time of time-invariant cognition across trials) Middle: A scatter plot of trial-averaged N200 peak-latencies and 10th reaction time percentiles. Observations were generated per noise condition and per EEG collection session ($N = 147$). Right: A scatter plot of single-trial N200 latencies versus single-trial reaction times. Observations were generated per trial ($N = 13{,}426$). Best-fit simple linear regression lines are shown in black with 95% confidence intervals for the intercept and slope parameters shown in gray. Overlaid on the linear regression lines are gold dashed lines representing the hypothesis with a slope of 1. That is, the expected influence of N200 peak-latency on reaction time is 1-to-1 millisecond if N200 peak-latency reflected human visual encoding time (VET).

Figure 5 Posterior distributions of effects of N200 peak-latency on NDT (Model 1). Posterior distributions provide measures of parameter uncertainty in Bayesian model-fitting methods. If the posterior distributions had most of their density around the blue line, this would be strong evidence for the 1-to-1 relationship when the model assumptions are true. Posterior distributions centered on the red line would be strong evidence for the null hypothesis (the effect parameter equals 0). Observations were generated per noise condition and per EEG collection session, resulting in 147 observations used in the linear model of trial-averaged N200 peak-latency on NDT embedded in a hierarchical decision-diffusion model. Some evidence exists for the effects of N200 peak-latency on NDT to be 1-to-1 (one millisecond increase in N200 peak-latency corresponds to a millisecond increase in NDT) as indicated by the Bayes Factors calculated with a Savage-Dickey density ratio (Verdinelli and Wasserman, 1995) of the posterior density over the prior distribution at $\gamma = 1$.

Figure 6 Session-level moderator effects (posterior distributions) of N200 peak-latency on NDT during the training experiment (Model 2). Observations were generated per noise condition and per EEG collection session, resulting in 147 observations used in the linear model of trial-averaged N200 peak-latency on NDT embedded in a hierarchical decision-diffusion model. The tests for moderator effects were inconclusive. Not much evidence exists for moderator effects of condition. There is also not much evidence for *no* moderator effects as indicated by the Bayes Factors for the null effects BF near 1 (e.g. there is not much evidence for $\theta = 0$, no effect of condition on the N200 and NDT relationship)

Figure 7 The addition of more trials with a contaminant (e.g. "mind-wandering") processes resulted in some non-decision time (NDT) estimates being negatively biased towards smaller values. This, in turn, resulted in decreased linear relationships (e.g. less than 1-to-1) between true NDT and estimated NDT. This was especially true for the hierarchical Bayesian estimates of simple decision-diffusion (DDM) model parameters, while the slopes between true NDT and 10th percentiles did not change much from 1-to-1 when more trials were added with a contaminant process. This suggested that while 10th percentiles were positively biased as estimates of true NDT (e.g. true NDT were approximately 60 milliseconds shorter than the 10th percentiles), the 1-to-1 relationship could be well estimated by the 10th percentiles but not the DDM fitting procedure when there were greater than 1% of trials with an unremoved contaminant process. This fact explains why a true measure of VET, such as the proposed N200 peak-latency, might not track DDM-estimated NDT well but would track 10th percentiles well.

Figure 8 Right and left sagittal and posterior views of localized trial-averaged N200 waveforms averaged across all EEG recordings and conditions ($N = 147$). Current Source Density MNI scalp topographies (Top) were generated with a Laplacian transform of EEG data (a projection of the first SVD component) with spline-interpolation between electrodes (Nunez and Pilgreen, 1991; Deng et al., 2012; Kayser and Tenke, 2015) . The cortical maps (Bottom) were obtained by projecting the MNI-scalp spline-Laplacians onto one subject's anatomical fMRI image via Tikhonov (L2) regularization, maintaining similar distributions of activity of the surface Laplacians on the cortical surface. Blue and

orange regions correspond to cortical areas estimated to produce negative and positive potentials observed on the scalp respectively. This localization suggests N200 activity occurs as a result of segregation of the target from visual noise due to the parietal and temporal locations suggesting activation of the "segregation pathway" (Mishkin et al., 1983; Lamme and Roelfsema, 2000). However variance in assumptions necessary for EEG localization across algorithms would yield diverse conclusions about the localization of this N200 activity (Nunez and Srinivasan, 2006).

Figure 9 A graphical illustration of a Neural Decision Diffusion model in which the encoding time τ_e on single-trials describes the latency of the negative peaks of the N200 waveform on 146 experimental trials. Single-trial observations of the N200 peak-latency are found by using a decomposition of the average ERP response at each electrode and then biasing the raw EEG by the resulting channel weights. Total NDT τ reflects both visual encoding time (VET) τ_e as well as residual motor response τ_m (i.e. motor preparation time after the decision is made) and can be estimated from reaction time distributions. Decision time is generated via a Brownian motion evidence accumulation process with evidence accumulation rate δ (drift rate), evidence accumulation noise ς (diffusion coefficient), and evidence threshold (boundary parameter) α (for more information see Ratcliff, 1978; Ratcliff and McKoon, 2008; Nunez et al., 2015, 2017)